Chemistry–A European Journal
Research Article
doi.org/10.1002/chem.202201178
Chemistry Europe
European Chemical Societies Publishing
www.chemeurj.org

Aggregation Modes of Chiral Diketopyrrolo[3,4-*c*]pyrrole Dyes in Solution and Thin Films

Gianluigi Albano,[a] Francesco Zinna,[b] Francesco Urraci,[b] Maria Annunziata M. Capozzi,[a] Gennaro Pescitelli,[b] Angela Punzi,*[a] Lorenzo Di Bari,*[b] and Gianluca M. Farinola[a]

Abstract: The chiroptical features of chiral diketopyrrolo[3,4-*c*]pyrrole (DPP) derivatives have been only marginally investigated to date. In this regard, we have synthesized *ad hoc* four chiral DPP dyes, functionalized with enantiopure alkyl groups from natural sources either on the lactam moieties or on the terminal positions of the π-conjugated backbone, to promote an efficient self-assembly into chiral supramolecular structures. For each of them, the aggregation modes has been investigated by absorbance and ECD spectroscopies in conditions of solution aggregation and on thin films, considering the effects of deposition technique (drop casting vs. spin coating) and post-deposition operations (solvent and thermal annealing). The effect of the structure of lateral π-conjugated units attached to the central DPP scaffold, as well as that of the position of the alkyl chiral group, has been assessed. ECD revealed superior capability, compared to absorbance spectroscopy, to provide information on the aggregation modes and to detect the possible co-existence of multiple aggregation pathways.

Introduction

The development of organic electronics is largely based on the design and synthesis of π-conjugated polymers and molecules, which are easily processable and exceptionally tuneable,[1] used as efficient active layers of devices such as organic field-effect transistors (OFETs)[2] or organic light-emitting diodes (OLEDs).[3] One of the most appealing features of organic π-conjugated systems compared to traditional inorganic semiconductors is that their intrinsic physico-chemical properties (absorbance and fluorescence, electron delocalization, HOMO-LUMO gap, charge and exciton transport, etc.)[4] can be finely tuned for the desired technological application by tailoring their molecular structure. At the same time, such properties are largely dependent on the solid state organization at different hierarchical levels, from the first-order supramolecular arrangement[5] up to the mesoscopic scale.[6] In this respect, π-conjugated system are often characterized by competing aggregation pathways during thin film preparation, leading to polymorphic local aggregated phases (e.g. kinetic vs. thermodynamic states) featuring different optoelectronic properties.[7] Mastering this feature is of paramount importance to obtain reproducibly the desired properties from the same materials.

The control of aggregation states of π-conjugated systems in thin films is crucial for the technological development of devices based on active layers of organic semiconductors. In this context, a privileged role is played by chirality: the introduction of stereodefinite chiral elements in π-conjugated molecules can drive their organization at all hierarchical levels and can prevent undesirable disordered structures.[8] Furthermore, in chiral supramolecular architectures, such as helices, spirals or chiral sheets, the perfect parallel and co-facial stacking between adjacent π-conjugated units is prevented, which is often desirable, for example to ensure longer exciton lifetime.[9] The chirality of these first-order supramolecular structures is often transferred to a larger scale, with the generation of twisted ribbons, helical fibers and other typical chiral nano/mesoscopic local textures.[10] Moreover, molecular and structural chirality opens the way to innovative technological applications: detection and production of circularly polarized (CP) light,[11] enantiopure chiral magnets,[12] optical information storage and processing,[13] chirality-induced spin selectivity (CISS),[14] enantioselective (electro)chemical sensing,[15] and so on.

Electronic circular dichroism (ECD) represents a fundamental technique for the characterization of chiral π-conjugated systems in solution and thin films, for clarifying and also predicting their structure-property relationship.[8] ECD signals are particularly sensitive to the arrangement of adjacent chromophores, providing information about the first level of supramolecular organization at the nanometric scale.[16] More

[a] *Dr. G. Albano, Prof. M. A. M. Capozzi, Prof. A. Punzi, Prof. G. M. Farinola*
Dipartimento di Chimica
Università degli Studi di Bari "Aldo Moro" Via Edoardo Orabona 4, 70126 Bari (Italy)
E-mail: angela.punzi@uniba.it
Homepage: https://www.farinolagroup.com/

[b] *Dr. F. Zinna, F. Urraci, Prof. G. Pescitelli, Prof. L. Di Bari*
Dipartimento di Chimica e Chimica Industriale
Università di Pisa
Via Giuseppe Moruzzi 13, 56124 Pisa (Italy)
E-mail: lorenzo.dibari@unipi.it
Homepage: https://ricerca.dcci.unipi.it/cd-pisa.html

Supporting information for this article is available on the WWW under https://doi.org/10.1002/chem.202201178

importantly, ECD can be applied seamlessly from solution to solid films, passing through intermediate aggregation states, providing a tool able to discriminate and recognize structures, which would appear indistinguishable to non-polarized light investigation.[7a] The development of sophisticated computational models often provides further insight into the structure-property relationship of such systems.[17]

However, it is worth to emphasize that ECD measurements on thin film samples are typically more complex than for isotropic solutions, due to the potential interference of macroscopic anisotropies often present in the solid state, i.e., linear dichroism (LD) and linear birefringence (LB), which may provide a significant contribution to the measured ECD spectrum.[18] The experimental ECD signals for a thin film can be expressed as the sum of several contributions, two of which are definitely the most significant: (i) an intrinsic isotropic component, i.e., the *reciprocal* CP absorption (named CD_{iso}), which is invariant upon sample orientation; (ii) a *non-reciprocal* CP absorption contribution (named LDLB), that is, an almost complete inversion of the handedness of CP component preferentially transmitted by the two opposite faces of the sample. This term arises from the combined effect of LD and LB′ (birefringence on an axis 45° offset from LB), resulting in the inversion of its sign by sample flipping (i.e., rotating the film by 180° with respect to its axis normal to the propagating light direction).[8,19] The reciprocal and non-reciprocal CP absorption of thin films of a chiral π-conjugated system represent the chiroptical response of two different scales of chirality: CD_{iso} is independent on the orientation and thus can be related to molecular and supramolecular chirality, for this reason it can exist in isotropic solution and possibly be transferred directly onto the thin film; on the contrary LDLB can only occur in structures, where a superior (polar) order is imparted by the surface where the sample is laid upon, reminiscent to what occurs in ferroelectric liquid crystals.[8]

In the last years, we have studied in detail the chiroptical properties of thin films of several chiral organic π-conjugated dyes: (arylenethienylene)s with benzo[1,2-*b*:4,5-*b*′]dithiophene, 9*H*-carbazole and 1,4-phenylene cores bearing chiral appendages easily prepared in enantiopure form from natural sources (chiral pool).[20] In particular, we found that they can actually give rise to several different supramolecular structures, with ECD features due to reciprocal CD_{iso} and non-reciprocal LDLB that are dependent on the nature of the chiral pendant group, the length of π-conjugated backbone, and the deposition technique (drop casting vs. spin coating).[19b,20b] We also proposed a simple and practical tool to recognize and quantify the relative weights of CD_{iso} and LDLB in the experimental ECD spectrum of a thin film, by taking, respectively, the semi-sum and the semi-difference of the ECD recorded for the front side (organic layer facing on the light source) and the back side (organic layer facing on the detector).[19b,20b] The two terms are given in Equations (1) and (2):

$$CD_{iso} = {}^1/_2 \times (ECD_{front} + ECD_{back}) \quad (1)$$

$$LDLB = {}^1/_2 \times (ECD_{front} - ECD_{back}) \quad (2)$$

Recognizing and quantifying both CD_{iso} and LDLB contributions in the ECD spectrum of a thin film of chiral organic π-conjugated systems can provide useful information on their solid-state organization at different hierarchy levels, which can help in the preparation of active layers of devices with the desired optoelectronic features.[8]

1,4-Diketo-3,6-diarylpyrrolo[3,4-*c*]pyrroles (DPPs) are a class of dyes with excellent photo and thermal stability,[21] used as pigments in paints, varnishes and plastics.[22] Due to their simple synthesis, high fluorescence quantum yield and good charge transport properties,[23] DPP derivatives have been widely explored as functional materials with applications ranging from organic electronics[24] to sensing and bioimaging.[25] The DPP core is a π-conjugated planar bicyclic structure containing two strong electron-withdrawing lactam groups, which can be easily functionalized by alkylation on the nitrogen atoms and by Pd-catalyzed coupling reactions on the (hetero)aryl groups at positions 3 and 6. The variation in the π-conjugation length or in the *N*-substitution has a large impact on DPPs self-assembly and, in turn, on their solid-state photo-physical properties,[26] while the influence of chains on terminal positions of the conjugated backbone has been less investigated.[27] In this context, we recently reported that by varying the length and the polarity of solubilizing groups on the lactam moieties or the terminal positions of π-conjugated backbone it is possible to induce the formation of *H*- or *J*-aggregates in triazole-DPP derivatives,[28] while the peripherical thioester functionalization can trigger the formation of near infrared-emitting *J*-aggregates in both bithiophene-DPP thin films and organic nanoparticles.[29]

The effect of chiral groups on the supramolecular self-assembly of DPP-based systems has been only marginally investigated to date. The attachment of helicene,[30] binaphthyl,[31] and pyrido-fused myrtanyl[32] enantiopure units on the terminal positions of π-conjugated backbone has been used as a strategy to obtain chiral DPP derivatives showing chiroptical features in solution and/or thin films. Chiral appendages on the lactam moieties of the DPP unit have been less investigated: only in two studies, reported by Kirkus et al.[26a] and by Würthner et al.,[33] DPP dyes *N*-substituted with chiral alkyl chains were synthesized and characterized in both solution and thin films by several techniques, but surprisingly no chiroptical spectroscopies were used. Therefore, the aggregation modes of chiral diketopyrrolo[3,4-*c*]pyrrole dyes in solution and thin films by chiroptical techniques, are still almost unexplored.

In this work, we report the synthesis of four new chiral 1,4-diketo-3,6-dithienylpyrrolo[3,4-*c*]pyrroles dyes **1**–**4**, functionalized with enantiopure alkyl groups from natural sources on the lactam moieties or the terminal positions of π-conjugated backbone, in order to study the effect of chirality on their aggregation modes by ECD spectroscopy in different conditions of solution aggregates and thin films (Figure 1). On the one hand, we designed a set of DPP dyes **1**–**3**, functionalized with

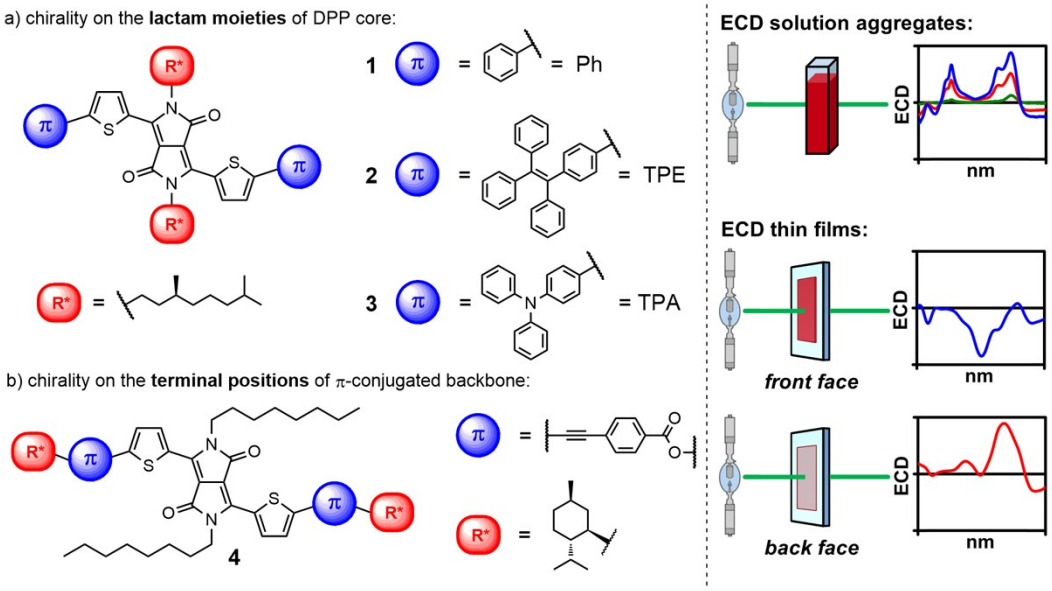

Figure 1. Scope of the work: four new chiral 1,4-diketo-3,6-dithienylpyrrolo[3,4-*c*]pyrroles dyes **1**–**4** (on the left), functionalized with enantiopure alkyl groups from natural sources on the lactam moieties or the terminal positions of π-conjugated backbone, have been synthetized in order to study the impact of chirality on their aggregation modes by ECD spectroscopy in different conditions of solution aggregation and thin films (on the right).

suitable π-conjugated units (phenyl, 4-(diphenylamino)phenyl, tetraphenylethylene) attached to the two lateral thiophene rings, and bearing the 3,7-dimethyl-1-octyl alkyl chain as chiral element on the lactam moieties. The introduction of such lateral π-conjugated units was performed in order to increase the self-assembly of DPP dyes through intermolecular π-stacking interactions between proximate molecules. The (*S*)-3,7-dimethyl-1-octyl chain is a chiral moiety prepared from natural (−)-β-citronellol,[34] a compound occurring in Nature in rose oils and *Pelargonium geranium*;[35] it is devoid of functionalities and it transfers its molecular asymmetry (stereogenic centre at position 3 of the aliphatic chain) to the entire system (chirality at supramolecular and mesoscopic scale) exclusively through dispersion forces and steric effects. On the other hand, we also designed the DPP dye **4**, which is instead characterized by two menthyl chiral units on the terminal positions of π-conjugated backbone, attached to the thiophene rings of central DPP core through a π-conjugated 4-ethynylbenzoate linkage. The enantiopure (1*R*,2*S*,5*R*)-menthyl scaffold, available from the natural monoterpenoid (−)-menthol (which is present in Nature in corn mint and peppermint oils),[36] is a bulky chiral alkyl moiety which may lead to a reduced torsional freedom of the π-conjugated system, thus facilitating the formation of chiral supramolecular aggregates.[37] The aggregation modes of chiral DPP dyes **1**–**4** were evaluated by absorbance and ECD in conditions of solution aggregation and thin films, considering the effect of deposition techniques (drop casting vs. spin coating) and post-deposition operations (solvent and thermal annealing). A comparative study of the impact on the chiroptical properties of the nature of lateral π-conjugated units and of the position of the alkyl chiral appendages was also performed: in this context, ECD measurements reveal valuable information that one would not obtain by using the sole absorbance spectroscopy.

Results and Discussion

The synthetic procedure developed for the preparation of chiral DPPs **1**–**4** is depicted in Scheme 1. For the first family of dyes, namely those bearing the chiral side chains on the lactam moieties of the central core, the synthesis was carried out starting from commercially available 1,4-diketo-3,6-dithienylpyrrolo[3,4-*c*]pyrrole **5** through an easy two-step procedure. First of all, **5** was alkylated with enantiopure (*S*)-1-bromo-3,7-dimethyloctane (**6**) using K_2CO_3 (3.3 equiv.) as the base at 130 °C in DMF as the solvent, and in the presence of a small amount of 18-crown-6 as a phase transfer catalyst[26a] to give the corresponding bis-alkylated product **7** in 61 % yield. Such intermediate was then subjected to a Pd-catalyzed direct C–H bond arylation reaction[38] with a slight excess (2.5–3.2 equiv.) of the suitable bromoarene (Ph–Br, TPE–Br or TPA–Br), in the presence of $Pd(OAc)_2$ (6–10 mol %) as the catalyst, K_2CO_3 (2.5 equiv.) as the base and pivalic acid (30 mol %) as the additive, in DMA at 110 °C for 2–3 h, affording the final chiral DPP dyes **1**–**3** in satisfactory yields (58–70 %). The synthesis of DPP **4**, bearing the chiral appendage on the two terminal positions of π-conjugated backbone, was carried out from (−)-menthyl 4-iodobenzoate (**8**)[39] via a three-step procedure. First, a Sonogashira coupling of **8** with trimethylsilylacetylene (**9**), performed with $PdCl_2(PPh_3)_2$ (3.3 mol %) and CuI (5.8 mol %) as the catalytic system, in a THF/Et_3N (1 : 1 v/v) mixture, afforded the TMS-protected alkyne **10** in high yield (90 %), which was then desilylated by treatment with an excess

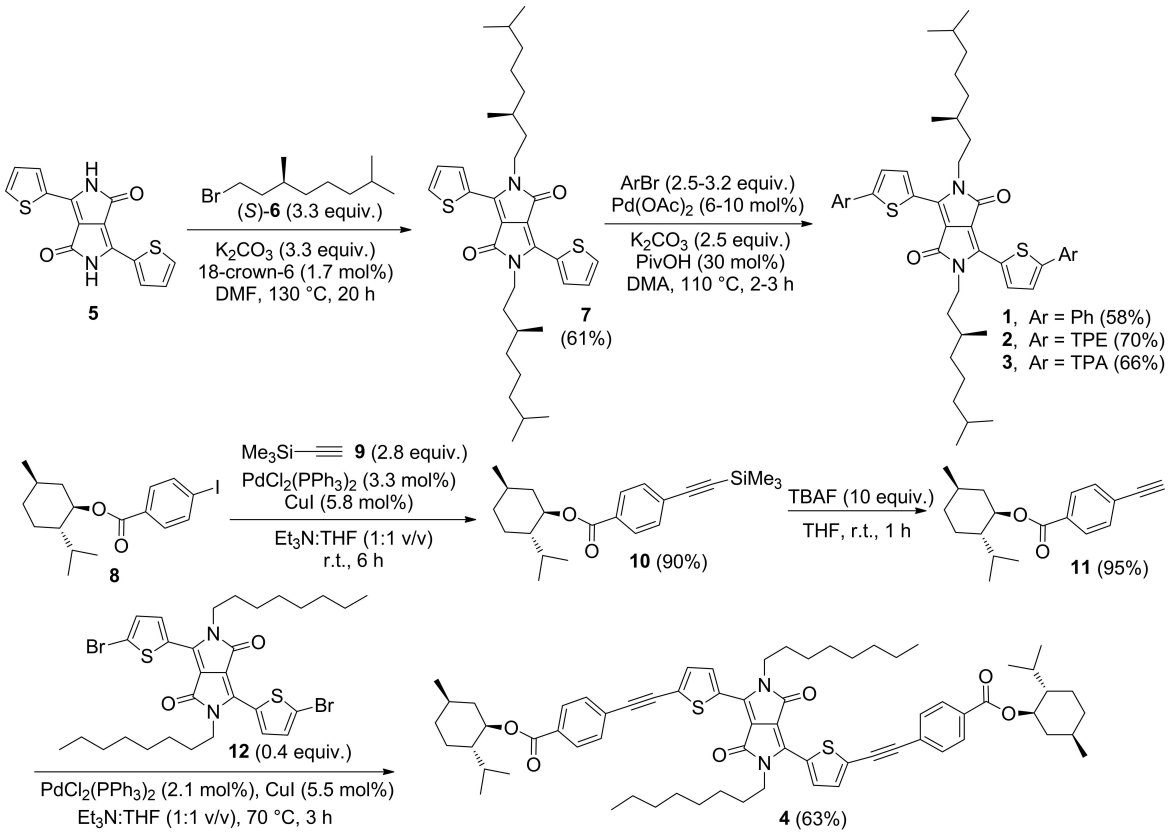

Scheme 1. Synthetic scheme developed for the preparation of chiral DPP dyes **1**–**4**: yields of pure products are reported in brackets.

of tetrabutylammonium fluoride in THF at room temperature for 1 h, giving (−)-menthyl 4-ethynylbenzoate (**11**) in 95% yield. The final step was a Sonogashira coupling of **11** with the dibrominated DPP compound **12** (which was synthesized according to the literature):[40] working at 70 °C in THF/Et_3N (1 : 1 v/v), with $PdCl_2(PPh_3)_2$ (2.1 mol%) as the catalyst and CuI (5.8 mol%) as the co-catalyst, the final chiral DPP dye **4** was obtained in 63% yield.

At first glance, all the final DPP compounds have the aspect of powder, dark purple or dark purple-blue solids, with no photoluminescence at different excitation wavelengths. In general, they showed good solubility in chlorinated solvents (i.e., CH_2Cl_2 and $CHCl_3$), while in non-polar solvents (such as *n*-hexane and toluene) and protic polar solvents (in particular, methanol and water) their solubility was quite low.

We started our investigation on chiral DPP dyes **1**–**4** with the study of their aggregation modes in different conditions of solution aggregation, induced by the use of solvent mixtures consisting of a *good* solvent (chloroform) and a *poor* solvent or non-solvent (methanol) in different ratio, by absorbance and ECD spectroscopies (Figure 2). In fact, spectral profiles obtained by the progressive addition of a non-solvent can give a step-by-step picture of the aggregation process. It is worth to emphasize that a similar study cannot be performed by emission spectroscopies: a strong fluorescence for DPPs **1**–**4** was observed in solution only as isolated molecules, while it was totally quenched for their solution aggregates apparently due to an aggregation-caused quenching (ACQ) effect.

We started our investigation with chiral DPP dyes **1**–**3**, bearing enantiopure (*S*)-3,7-dimethyl-1-octyl chains on the lactam moieties of the central core. The structurally simplest system belonging to this family of dyes is **1**, functionalized with phenyl units on the two lateral thiophene rings. The absorbance spectrum of **1** in $CHCl_3$ solution (Figure 2a, black line) showed a broad band between 450 nm and 650 nm characterized by a clear vibronic structure, with maximum at 596 nm ($\varepsilon = 1.24 \cdot 10^5\ M^{-1}\ cm^{-1}$). In the literature, this band has been attributed to an intramolecular charge-transfer transition from the thiophene rings to the DPP moiety.[41] With the purpose of verifying this statement, we run time-dependent DFT (TD-DFT) calculations on a model "isolated" chromophore (the *N,N*-dimethyl analogue of **1**). Our calculation results demonstrate this is a rather local $\pi \rightarrow \pi^*$ transition, with negligible CT character (Figure S1 in Supporting Information). The vibrational structure associated with this band has spacings of 1100–1300 cm^{-1} (Figure S2), compatible with aromatic ring stretching vibrations. At higher energy one finds a more structured band attributable to a second $\pi \rightarrow \pi^*$ transition of the π-conjugated backbone, with maxima at 391 nm ($\varepsilon = 3.81 \cdot 10^4\ M^{-1}\ cm^{-1}$) and at 333 nm ($\varepsilon = 8.14 \cdot 10^4\ M^{-1}\ cm^{-1}$). Since DPP dye **1** is well soluble in chlorinated solvents, the absorbance spectrum in Figure 2a described the situation of molecularly dispersed non-

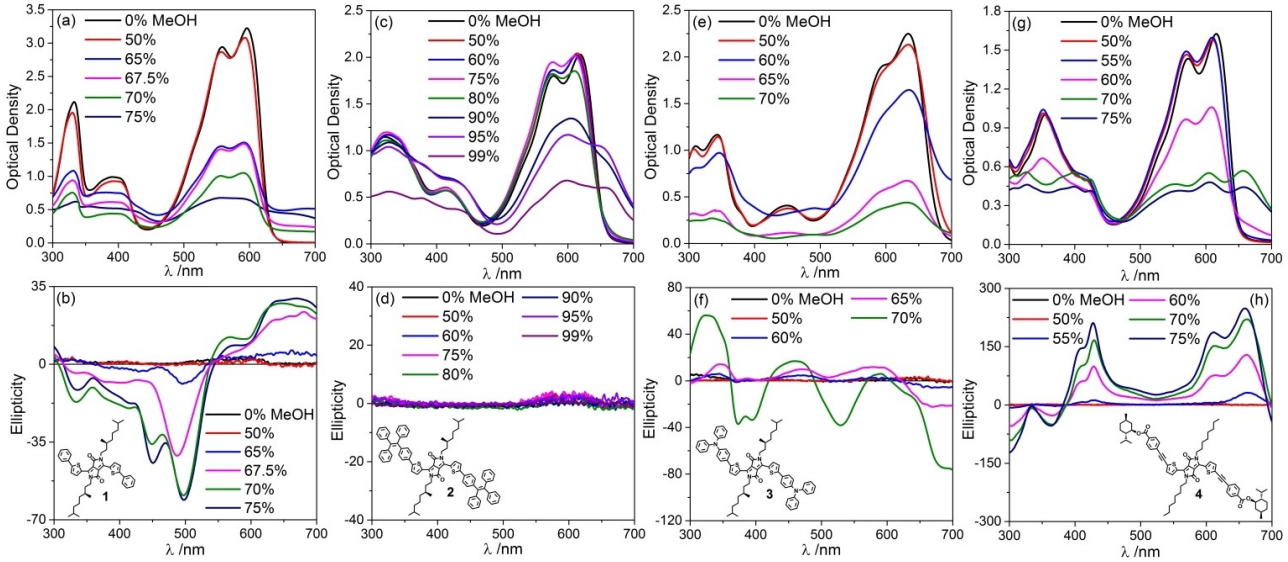

Figure 2. Optical and chiroptical study of the aggregation modes of chiral DPP dyes **1**–**4** in conditions of solution aggregation. Absorbance spectra of **1** (a), **2** (c), **3** (e) and **4** (g) in $CHCl_3$/MeOH mixtures with increasing amounts of MeOH. ECD spectra of **1** (b), **2** (d), **3** (f) and **4** (h) in $CHCl_3$/MeOH mixtures with increasing amounts of MeOH. Sample concentration: $1.3 \cdot 10^{-5}$ M.

aggregated species. This was confirmed by the corresponding ECD spectrum (Figure 2b, black line), where no significant signals were found, indicating that the perturbation exerted on the intrinsically achiral π-conjugated chromophore of DPP dye **1** by individual chiral centres of the two (*S*)-3,7-dimethyl-1-octyl moieties is very small in dissolved molecules. A gradual increase in the amount of methanol as the *poor* solvent led to the formation of supramolecular aggregates. In particular, in the absorbance spectra of **1** recorded for $CHCl_3$/MeOH mixtures (Figure 2a) starting from 65% MeOH we observed a gradual hypochromism, which is a first important indication of supramolecular self-assembly. The corresponding ECD spectra in $CHCl_3$/MeOH mixtures (Figure 2b) provided an unequivocal proof of the occurrence of solution aggregates: a weak structured ECD signal appeared at 65% MeOH, described as an asymmetric positive exciton couplet,[16d] which increased gradually in intensity by further addition of the *poor* solvent up to 75% MeOH, where it showed maximum dissymmetry factors g_{abs} (defined as $\Delta\varepsilon/\varepsilon$ or $\Delta A/A$) of $+2.1 \cdot 10^{-3}$ at 669 nm and $-4.2 \cdot 10^{-3}$ at 498 nm. The positive ECD couplet suggested the occurrence of a right-handed supramolecular helix, held together by the twisted π-stacking of aromatic units with a well-defined helicity, induced by the enantiopure alkyl moieties through ancillary interactions (non-polar forces and steric effects). It is worth to emphasize that such ECD profiles were also invariant as a function of time (about 1 h), thus indicating a thermodinamically stable aggregation mode. However, a further increase in the amount of the *poor* solvent (that is, above 75% MeOH) caused a precipitation of **1** from the solution.

The tetraphenylethylene (TPE) unit is a typical structural motif in π-conjugated systems, often used as an aggregation-induced emission luminogen (AIEgen), with a remarkable self-assembly ability in solution thanks to the formation of strong intermolecular π-stacking interaction between proximate units favoured by its rigid structure.[42] These peculiar features of the TPE unit clearly influenced the optical and chiroptical properties of DPP dye **2** in solution, although it should be emphasized that also in this case the emission of its solution aggregates was totally quenched, due to a significant ACQ effect which was not prevented by the TPE units. The absorbance spectrum in $CHCl_3$ (Figure 2c, black line) showed the main broad band at lower energy than **1**, ranging between 470 nm and 650 nm, with a vibronic structure and maximum at 618 nm ($\varepsilon = 7.81 \cdot 10^4\ M^{-1}\ cm^{-1}$), and a further structured band at higher energy, with maxima at 413 nm ($\varepsilon = 2.32 \cdot 10^4\ M^{-1}\ cm^{-1}$) and at 322 nm ($\varepsilon = 4.41 \cdot 10^4\ M^{-1}\ cm^{-1}$). A first significant difference compared to DPP dye **1** was observed in the spectra recorded for $CHCl_3$/MeOH mixtures. By increasing the amount of the non-solvent, from 90% MeOH we found a more substantial solvatochromism: the structured band in the higher energy region was slightly red-shifted, while for the band at lower energy a shoulder appeared at 655 nm (the so-called "aggregation band"),[42] which increased rapidly in intensity by further addition of the *poor* solvent up to 99% MeOH. All these changes in the absorbance spectrum offered an unequivocal proof of the occurrence of solution aggregates: on the one hand, aggregation induces an increased planarization of two lateral TPE-thienylene units which causes the slight red-shift of the pristine absorbance band associated to the $\pi \rightarrow \pi^*$ transition; on the other hand, the shoulder appeared at 655 nm is a typical manifestation of self-assembly of DPP moieties, promoted by the π-stacking interactions between proximate aromatic TPE units favoured by their close to planarity and rigid structure. However, a very unexpected behaviour was observed in the corresponding ECD spectra (Figure 2d): no significant signals were found not only in pure chloroform, but also in

$CHCl_3$/MeOH mixtures with high amounts of methanol. Such results could be reasonably explained by hypothesizing a self-assembly of **2** into achiral, ordered supramolecular structures, where the perfect co-facial stacking of adjacent molecules is preferred compared to a helical twisted one. In particular, a possible explanation is that the weak non-polar interactions and steric effects exerted by the enantiopure (*S*)-3,7-dimethyl-1-octyl moieties are unable to induce a twist between adjacent π-conjugated chromophores, held together by the strong co-facial intermolecular π-stacking interaction of TPE units, thus favouring an achiral ordered stacking.

The triphenylamine (TPA) unit represents a very useful electron-rich core, which can be linked to electron withdrawing groups in order to generate donor-acceptor systems, with several applications in organic optoelectronics.[43] Moreover, the TPA scaffold also manifests good self-assembly properties: despite its lower rigidity compared to TPE unit, the presence of three phenyl rings and an electron rich nitrogen atom offered several opportunities of non-covalent interactions. Therefore, it is not surprising that chiral DPP dyes **3** showed very appealing optical and chiroptical features. In pure $CHCl_3$, the absorbance spectrum (Figure 2e, black line) displayed a broad main band between 500 nm and 700 nm, with maximum at 634 nm ($\varepsilon = 8.65 \cdot 10^4\ M^{-1}\ cm^{-1}$) and a shoulder at 598 nm, and two other bands at higher energy, which can be attributed to the TPA-thienylene units, with maximum at 450 nm ($\varepsilon = 1.56 \cdot 10^4\ M^{-1}\ cm^{-1}$) and 343 nm ($\varepsilon = 4.48 \cdot 10^4\ M^{-1}\ cm^{-1}$). By the addition of methanol as the non-solvent, starting from 60% MeOH we observed a marked hypochromism of all the signals. The occurrence of self-assembly was confirmed by circular dichroism measurements (Figure 2f): from 60% MeOH, we observed a quite complex ECD profile consisting of several bands, whose intensities gradually increased with higher amounts of non-solvent up to 70% MeOH. Under these conditions of maximum solution aggregation (beyond which the unwanted precipitation of the material started), we found three negative bands centered at 734 nm ($g_{abs} = -2.6 \cdot 10^{-2}$), 529 nm ($g_{abs} = -9.5 \cdot 10^{-3}$) and 373 nm ($g_{abs} = -7.7 \cdot 10^{-3}$), and two positive bands at 459 nm ($g_{abs} = +6.6 \cdot 10^{-3}$) and 324 nm ($g_{abs} = +6.6 \cdot 10^{-3}$). The strong ECD signals observed for chiral DPP dye **3** in 70% MeOH suggest a sequence of negative exciton couplets.[44] Two crossover points, around 380 and 500 nm, closely match two maxima in the absorbance spectrum of the isolated molecules (below 60% MeOH). In the low-energy edge the situation appears less clear, possibly because of partial overlap with the higher energy transition but also more relevantly because of the appearance of aggregation bands, with no correspondence in the absorbance spectrum of the isolated molecule. These aggregation bands may be associated with an intrinsically chiral π-conjugated skeleton, which becomes twisted upon aggregation, leading to ECD contribution of a single sign (negative). Thus, the broad negative ECD band in the near IR would be the superposition of a negative exciton couplet of the 650 nm transition with another negative Cotton effect exquisitely stemming from the aggregated chromophores, thus suggesting a left-handed supramolecular chirality.

Although chiral DPP dyes **1**–**3**, bearing the same enantiopure (*S*)-3,7-dimethyl-1-octyl chains on the lactam moieties of the central core, only differed in the lateral π-conjugated units attached to the central DPP scaffold, we observed three very different situations in terms of solution aggregates: right-handed supramolecular helical structures, associated to a positive ECD couplet, in the case of Ph-functionalized chiral DPP dye **1**; achiral, ordered structures with co-facial stacking of adjacent molecules, associated to negligible ECD signals, for the TPE-functionalized chiral DPP dye **2**; left-handed supramolecular chirality, associated to a quite complex ECD spectrum shape, in the case of TPA-functionalized chiral DPP dye **3**.

We then focused our attention on the solution self-assembly of chiral DPP dye **4**, bearing two enantiopure (−)-menthyl appendages on the terminal positions of π-conjugated backbone. Compared to the 3,7-dimethyl-1-octyl branched chain, the menthyl group is a bulkier chiral cyclic moiety which can more easily lead to the formation of strong supramolecular aggregates in solution, thanks to a reduced torsional freedom of the π-conjugated system. The absorbance spectrum of **4** in pure $CHCl_3$ (Figure 2g, black line) showed the main broad band between 470 nm and 650 nm, due to the main π→π* transition of the DPP moiety, with maximum at 616 nm ($\varepsilon = 6.25 \cdot 10^4\ M^{-1}\ cm^{-1}$), and a further band due to the second π→π* transition between 450 nm and 300 nm, with maximum at 354 nm ($\varepsilon = 3.85 \cdot 10^4\ M^{-1}\ cm^{-1}$). This situation is associated with molecularly dispersed non-aggregated species, as confirmed by the weak signals of the corresponding ECD spectrum (Figure 2h, black line). The progressive increase in the amount of methanol caused a gradual change in the absorbance spectrum (Figure 2g): in addition to a general hypochromism, from 70% MeOH we observed the appearance of a new aggregation band centered at 659 nm, suggesting the occurrence of a significant supramolecular self-assembly. This feature is more evident in ECD measurements (Figure 2h): from 55% MeOH, a complex pattern of bands was found, whose intensities increased up to 75% MeOH, that is, the maximum added amount of non-solvent before solid precipitation. In these latter conditions, ECD consisted of an extended positive region between 400 nm and 700 nm, due to the partial overlap of two strong bands at 659 nm ($g_{abs} = +1.7 \cdot 10^{-2}$) and 427 nm ($g_{abs} = +1.6 \cdot 10^{-2}$), and two minor negative bands at 363 nm ($g_{abs} = -4.0 \cdot 10^{-3}$) and 300 nm ($g_{abs} = -8.9 \cdot 10^{-3}$), besides a pronounced long-wavelength tailing due to the scattering of suspended particles, which is a further confirmation of the presence of solution aggregates. In relation with the above discussion of the ECD of **3**, here we may tentatively recognize a *positive* ECD couplet in the higher energy region, with crossover around 390 nm, that may be associated with the 354 nm absorption band. The low-energy end is dominated here by the positive component, possibly allied to an intrinsic chiral skeleton reached after aggregation.

The optical and chiroptical study of chiral π-conjugated systems in solution by progressive addition of non-solvent affords step-by-step snapshots of the self-assembly processes which are expected to mimic the behaviour in the solid state. Therefore, the investigation of the solution aggregates is often

preparatory to their study in the solid state. In particular, the ability to recognize and control different aggregation modes in thin film samples would be useful for obtaining layers of chiral π-conjugated systems with tunable properties for innovative optoelectronic applications.[8] In light of these considerations, we then focused our attention to the investigation of the chiroptical properties of chiral DPP dyes **1**–**4** in thin films, prepared by drop casting (DC) or spin coating (SC) technique. For drop-casted samples, ~200 μL of a CH_2Cl_2 or $CHCl_3$ solution of each compound (concentration: $2.0 \cdot 10^{-3}$ M) were deposited on quartz plates, followed by slow evaporation of the solvent in a closed chamber saturated with CH_2Cl_2 or $CHCl_3$ vapours. Spin-coated samples were prepared by depositing ~100 μL of a CH_2Cl_2 or $CHCl_3$ solution of each compound (concentration: $2.0 \cdot 10^{-2}$ M) on quartz plates, followed by fast evaporation of the solvent, while spinning the plates (1000 rpm for 30 s). All the samples showed a thickness of roughly 100 nm and macroscopically appeared semi-transparent. The effect of two different post-deposition operations was also evaluated: solvent annealing, carried out by keeping samples for 1 h in a closed chamber saturated with solvent vapours; thermal annealing, performed by keeping samples for 1 h in an oven at 100 °C.

Thin films were first characterized by optical microscopy (Figure S3–S10). In all cases, crater-like features with diameters from 150 to 250 μm were detected for freshly prepared thin film samples, which in some cases showed a texture evolution upon thermal and solvent annealing. It is noteworthy that polarized microscopy (POM) images did not reveal any apparently birefringent domain.

For each thin film, absorbance and ECD spectra were measured; in particular, ECD was recorded for both front side and back side, in order to quantify the relative weights of reciprocal CD_{iso} and non-reciprocal LDLB contributions by taking, respectively, their semi-sum and semi-difference. It is worth to emphasize that only (chiro)optical features in transmission can be investigated for these samples; similarly to what explained above for solution aggregates, no emission was found in thin films due to a strong ACQ effect, thus preventing the collection of fluorescence and CPL spectra.

Once again, we started with chiral DPPs bearing enantiopure (*S*)-3,7-dimethyl-1-octyl chains on the lactam moieties of the central core. The optical and chiroptical investigation of the aggregation modes in thin films of compound **1**, bearing the simple Ph lateral π-conjugated units attached to the central DPP core, is depicted in Figure 3. The drop-casted sample (**DC-1**) showed an absorbance spectrum (Figure 3a) roughly similar to the solution spectrum, with a broad band at lower energy, between 470 nm and 700 nm, attributable to the main π→π* transition, and a structured band in the higher energy region (300–450 nm) due to the second π→π* transition of π-conjugated backbone. The most relevant difference with respect to solution is the appearance of a shoulder at 650 nm: this is a typical sign of the strong interaction between π-conjugated units of proximate molecules occurring in the solid state. The ECD profiles recorded for the front and the back (Figure 3b) were quite similar, although not perfectly coincident, suggesting a predominant reciprocal CD_{iso} contribution. In particular, a complex pattern of signals was observed: positive bands at 735 nm (g_{abs} front: $+2.5 \cdot 10^{-2}$; back: $+1.8 \cdot 10^{-2}$), 518 nm and 319 nm, and negative bands at 602 nm and 355 nm; the band at 470 nm is noticeable, since a signal inversion upon sample flipping was found (g_{abs} front: $+4.7 \cdot 10^{-4}$;

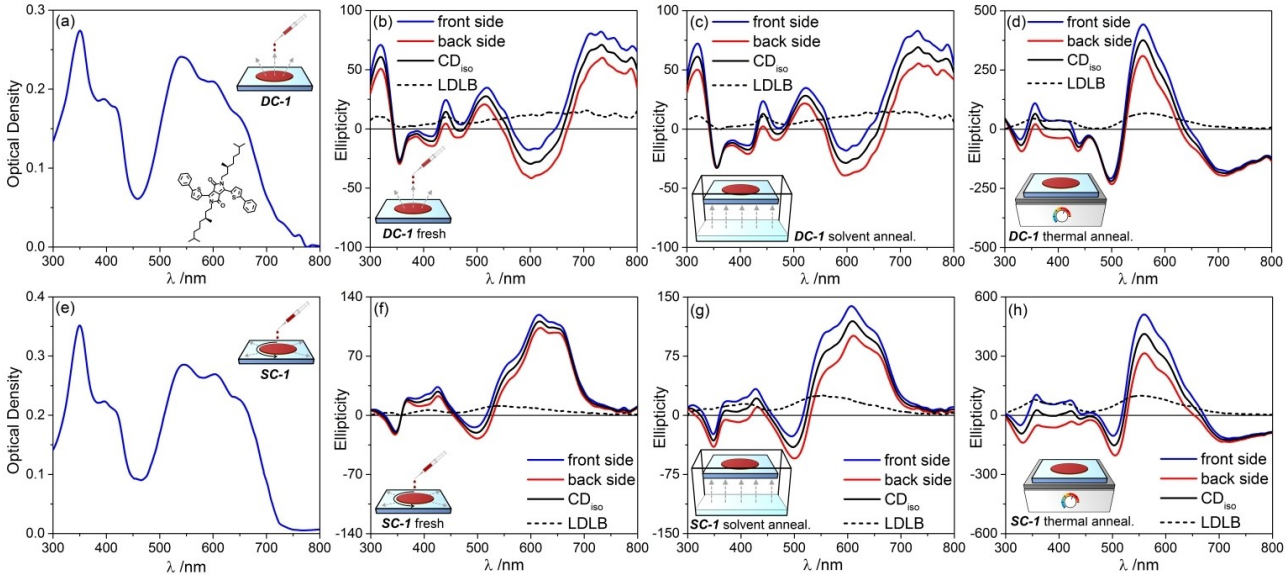

Figure 3. Optical and chiroptical investigation of the aggregation modes of chiral DPP dye **1** in thin films. Absorbance spectra recorded for: drop-casted sample **DC-1** (a); spin-coated sample **SC-1** (e). ECD spectra (normalized with respect to maximum absorbance) recorded for: drop-casted sample **DC-1** freshly prepared (b), after solvent annealing (c) and after thermal annealing (d); spin-coated sample **SC-1** freshly prepared (f), after solvent annealing (g) and after thermal annealing (h). For each panel: blue line is the ECD spectrum recorded for the front face; red line is the ECD spectrum recorded for the back face; black continuous line is the front-back semi-sum, i.e., calculated CD_{iso} contribution; black dashed line is the front-back semi-difference, i.e., calculated LDLB contribution.

back: $-8.9\cdot10^{-4}$). In this sample the LDLB contribution is very low: the minimal changes in the ECD signals observed for the two faces of thin films were actually due to reproducibility issues related to an off-set of the sample, and possibly associated with dispersive phenomena, rather than to non-reciprocal effects in the CP absorption. This means that the experimental ECD spectrum can be considered as the result of a substantial CD_{iso} term due to supramolecular chirality. It is noteworthy that the shape of the thin film ECD spectrum was quite different from that observed in $CHCl_3$/MeOH solutions: we could hypothesize the occurrence of a different aggregation pathway with respect to solution self-assembly, which would be very difficult to identify by means of absorbance spectroscopy only. The ECD spectrum of **DC-1** after solvent annealing (Figure 3c) showed no changes, keeping the same shape and intensity. During the solvent annealing process, π-conjugated chains typically acquire greater mobility, thus allowing their rearrangement into a more thermodynamically stable aggregation state. This is not the case of **DC-1**, where the slow evaporation of the solvent was sufficient to allow the molecules to organize into a stable aggregation mode. However, thermal annealing of sample **DC-1** resulted in a significant change in the ECD spectrum (Figure 3d): although a great similarity of the ECD spectra recorded for the two faces of the sample was still observed, we also found a significant change in the spectral shape, associated to a general inversion of its sign with respect to freshly prepared **DC-1**. Moreover, a clear increase in the ECD signal intensities was found, with maximum g_{abs} value (708 nm) of $-2.7\cdot10^{-2}$ for the front side and of $-3.1\cdot10^{-2}$ for the back side. High temperature could favour the evolution of the sample towards a different thermodynamic aggregation state, presumably characterized by an opposite helicity and a more effective exciton coupling between adjacent π-conjugated chromophores.

Thin films of chiral DPP dye **1** prepared by spin coating technique (**SC-1**) showed an absorbance spectrum (Figure 3e) quite similar to **DC-1**, with a more prominent "aggregation shoulder" at 643 nm. The corresponding ECD spectrum (Figure 3f) revealed an almost perfect correspondence of the spectral profiles measured for the front and the back face, as confirmed by the low $\int|LDLB|/\int|CD_{iso}|$ ratio of 0.14 (where $\int|LDLB|$ and $\int|CD_{iso}|$ are, respectively, the integrated area for the absolute value of semi-difference and semi-sum ECD spectra). In particular, a strong positive band fell between 520 nm and 780 nm, with maximum at 615 nm (g_{abs} front: $+4.9\cdot10^{-3}$; back: $+4.2\cdot10^{-3}$), and three other less intense bands at 497 nm, 424 nm and 346 nm. Interestingly, such spectrum is similar to that observed for solution aggregates of DPP dye **1** in 75% MeOH, suggesting us a similar supramolecular organization. Spin coating is a fast deposition technique, where solution is very quickly spread and the solvent immediately evaporates, without the molecules having enough time to rearrange; therefore, we could reasonably assume that the aggregation modes in spin-coated samples represent a frozen situation of what occurs in the conditions of solution self-assembly. The effect of solvent annealing on **SC-1** did not produce a substantial change in the ECD spectrum (Figure 3g), while a more marked change in ECD was observed in **SC-1** sample after thermal annealing (Figure 3h): a profile very similar to that of thermally annealed **DC-1** (in terms of spectral shape, g_{abs} values and $LDLB/CD_{iso}$ ratio) was found. Therefore, the effect of high temperature is to promote the evolution of chiral DPP **1** towards the same thermodynamically stable aggregation state, regardless of the starting solid-state organization (**DC-1** or **SC-1**).

A different behaviour was observed in the chiro(optical) study of thin films of chiral DPP dye **2**, bearing lateral TPE π-conjugated units. The absorbance spectra of samples prepared by both drop casting (**DC-2**) and spin coating (**SC-2**) were very similar, with a broad band between 470 and 700 nm centered at 585 nm and a prominent shoulder at 630 nm, and a further structured band between 450 nm and 300 nm (Figures 4a and 4e). The appearance of the low-energy shoulder indicated the occurrence of strong interactions between π-conjugated backbones of proximate molecules, which was here particularly favoured by the presence of TPE units. However, the absorbance spectra did not provide structural information on these aggregation modes. The ECD measurements recalls the same phenomenon of $CHCl_3$/MeOH mixtures: both **DC-2** and **SC-2** pristine samples showed no signals (Figure 4b and Figure 4f, respectively). Even in the solid state, the weak hydrophobic forces and steric effects exerted by the enantiopure (*S*)-3,7-dimethyl-1-octyl moieties are apparently unable to create a twist between adjacent π-conjugated chromophores, held together by the strong co-facial intermolecular π-stacking of TPE units, favouring an achiral ordered aggregation mode. Thermal annealing of both **DC-2** and **SC-2** samples did not yield any variation in the ECD spectra (Figure 4d and Figure 4h, respectively): it is reasonable that the network of strong co-facial π-stacking of TPE units favoured a thermodynamically stable solid-state organization, which is not disrupted even by high temperatures. No significant structural rearrangement of thin films was observed even after solvent annealing: ECD spectrum of **DC-2** (Figure 4c) still showed the same aspect with no significant signals, while in the case of **SC-2** two weak bands of low intensity appeared (Figure 4g). In particular, in this last case it is worth to emphasize that the spectra recorded for the two faces of the sample were almost specular: two negative bands (584 nm, $g_{abs}=-2.3\cdot10^{-4}$; 322 nm, $g_{abs}=-7.0\cdot10^{-4}$) for the front, and two positive bands (596 nm, $g_{abs}=+1.9\cdot10^{-4}$; 309 nm, $g_{abs}=+2.4\cdot10^{-4}$) for the back. This indicates a predominant non-reciprocal LDLB contribution, although still associated with weak signal intensity, in the global ECD spectrum of **SC-2** ($\int|LDLB|/\int|CD_{iso}|=1.65$), suggesting a quite modest rearrangement of these achiral supramolecular aggregates into mesoscopic domains with a preferential orientation with respect to the glass slide surface.

Thin films of chiral DPP dye **3**, functionalized with TPA lateral units, showed the most interesting results, with a strong dependence of their chiro(optical) features as a function of the deposition technique and post-deposition curing (Figure 5). Concerning the sample fabricated by drop casting (**DC-3**), the absorbance spectrum (Figure 5a) showed a broad band between 500 and 750 nm, with maximum at 609 nm and the

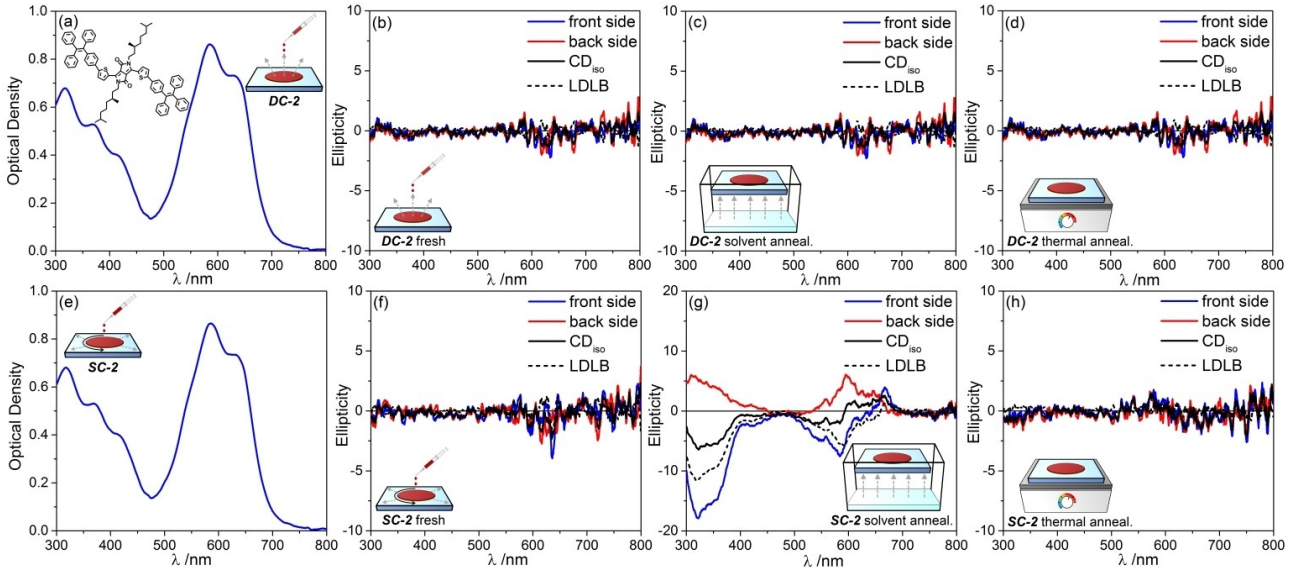

Figure 4. Optical and chiroptical investigation of the aggregation modes of chiral DPP dye **2** in thin films. Absorbance spectra recorded for: drop-casted sample **DC-2** (a); spin-coated sample **SC-2** (e). ECD spectra (normalized with respect to maximum absorbance) recorded for: drop-casted sample **DC-2** freshly prepared (b), after solvent annealing (c) and after thermal annealing (d); spin-coated sample **SC-2** freshly prepared (f), after solvent annealing (g) and after thermal annealing (h). For each panel: blue line is the ECD spectrum recorded for the front face; red line is the ECD spectrum recorded for the back face; black continuous line is the front-back semi-sum, i.e., calculated CD_{iso} contribution; black dashed line is the front-back semi-difference, i.e., calculated LDLB contribution.

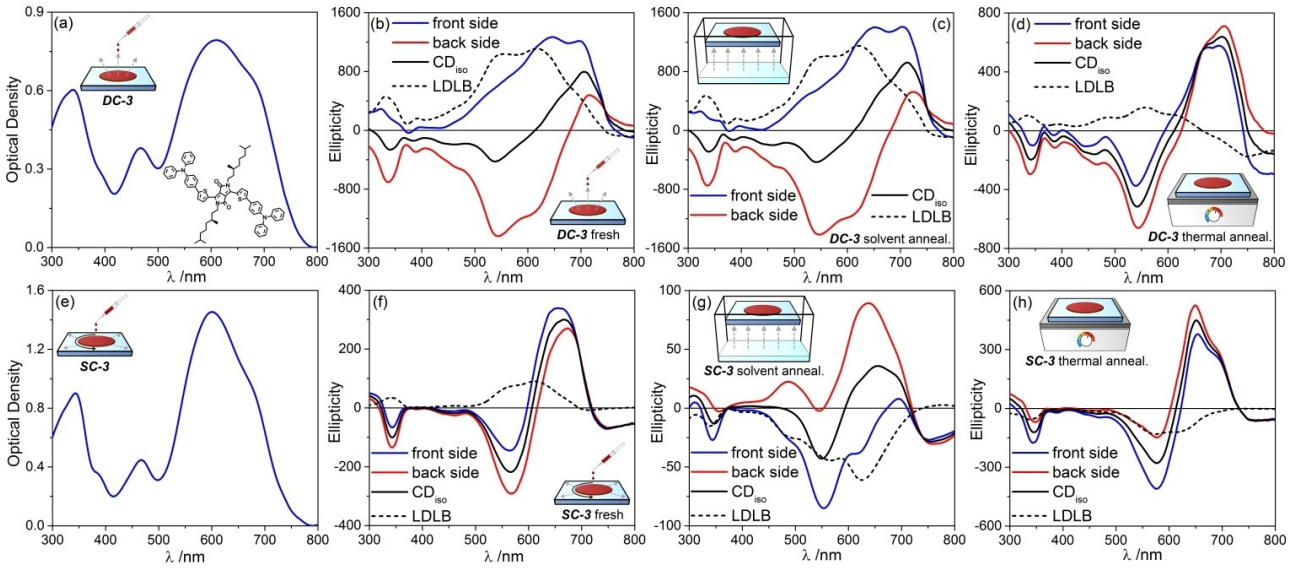

Figure 5. Optical and chiroptical investigation of the aggregation modes of chiral DPP dye **3** in thin films. Absorbance spectra recorded for: drop-casted sample **DC-3** (a); spin-coated sample **SC-3** (e). ECD spectra (normalized with respect to maximum absorbance) recorded for: drop-casted sample **DC-3** freshly prepared (b), after solvent annealing (c) and after thermal annealing (d); spin-coated sample **SC-3** freshly prepared (f), after solvent annealing (g) and after thermal annealing (h). For each panel: blue line is the ECD spectrum recorded for the front face; red line is the ECD spectrum recorded for the back face; black continuous line is the front-back semi-sum, i.e., calculated CD_{iso} contribution; black dashed line is the front-back semi-difference, i.e., calculated LDLB contribution.

typical shoulder at 680 nm, and two other less intense bands at higher energy, with maxima at 466 nm and 338 nm. Although such spectrum is roughly comparable to the one observed for solution aggregates, the large band-width and the presence of the shoulder at low energy suggested the occurrence of intermolecular interaction in the solid state. More information came from ECD measurements, where we observed substantial differences with respect to the other two DPP dyes belonging to the same family. In particular, from Figure 5 it is evident that, although all the experimental ECD spectra are quite different from each other, the shape of the CD_{iso} term appears very similar in all the samples, thus suggesting the existence of the

same first-order supramolecular organization. On the contrary, the variation of the LDLB term suggests the presence of different aggregation modes at mesoscopic level. In the case of freshly prepared **DC-3** sample, we found very strong ECD signals (with a maximum g_{abs} value almost 3-fold more intense than that of Ph-functionalized DPP **1** and about two orders of magnitude greater than TPE-functionalized DPP **2**), with a substantial inversion of the ECD signals upon sample flipping, although the spectral profiles recorded for the front and the back were not perfectly mirror image (Figure 5b). In particular, the ECD spectrum of the front face showed a broad positive band between 450 and 750 nm, with two peaks at 697 nm ($g_{abs} = +5.2 \cdot 10^{-2}$) and 647 nm ($g_{abs} = +4.2 \cdot 10^{-2}$), and a further positive small band at higher energy, with maximum at 323 nm ($g_{abs} = +1.2 \cdot 10^{-2}$); for the back, we found a broad negative band between 370 and 680 nm (maximum at 544 nm, $g_{abs} = -6.2 \cdot 10^{-2}$) and a small negative band at 337 nm ($g_{abs} = -2.8 \cdot 10^{-2}$), but also a further positive band at lower energy (717 nm, $g_{abs} = +2.9 \cdot 10^{-2}$). By taking the semi-sum and the semi-difference of these two spectra according to Equations (1) and (2), we clearly evidence a predominant non-reciprocal LDLB, confirmed by a $\int|\mathrm{LDLB}|/\int|\mathrm{CD_{iso}}|$ ratio of 1.96. The existence of a non-negligible CD_{iso} term, having the appearance of an asymmetric positive exciton couplet, suggested the organization of the molecules into right-handed supramolecular helical structures; their further organization into highly anisotropic mesoscopic domains, with a preferential orientation with respect to a surface, was instead responsible for the strong LDLB contribution.[19b] Similarly to **DC-1**, also in this case the ECD profiles recorded for both faces, as well as the resulting CD_{iso} term, were quite different from that observed in $CHCl_3$/MeOH solutions, indicating a different aggregation mode with respect to solution aggregates. The application of solvent annealing did not produce any significant changes in the ECD spectrum of **DC-3** (Figure 5c), which retained the same shape and intensity: the evaporation of the solvent during drop casting deposition was sufficiently slow to allow the molecules to organize into a relatively stable thermodynamic aggregation mode, without acquiring increased mobility as typically happens for π-conjugated chains during solvent curing. However, thermal annealing led to a substantial variation of the ECD spectrum (Figure 5d), allowing the system to reach the most thermodynamically stable aggregation state, characterized by a similar first-order supramolecular arrangement but a very different organization at mesoscopic level. In particular, by taking the semi-sum and the semi-difference of the profiles recorded for the front and the back face, we found a sharp decrease of the LDLB contribution, while CD_{iso} kept the same shape and intensity of the pristine **DC-3** sample ($\int|\mathrm{LDLB}|/\int|\mathrm{CD_{iso}}| = 0.38$). This result is very interesting: we hypothesize that the effect of high temperature is able to break the highly anisotropic mesoscopic domains responsible for non-reciprocal LDLB contribution, but without affecting the chiral supramolecular aggregates responsible for the reciprocal CD_{iso} term. Interestingly enough, the **DC-3** sample is that showing the more structured microscopy images (see Figure S7), especially after the solvent annealing treatment: a micro-texture with several crater-like features of μm-size is visible.

Thin film samples of DPP dye **3** fabricated by spin coating technique (**SC-3**) showed an absorbance spectrum (Figure 5e) similar to that of pristine **DC-3**, which could suggest a very similar solid-state organization. Actually, the ECD spectrum revealed a situation apparently similar to that of thermally annealed **DC-3**, rather than to the freshly-prepared sample (Figure 5f): a substantial correspondence of the profiles recorded for the two faces was found, due to a predominant reciprocal CD_{iso} term ($\int|\mathrm{LDLB}|/\int|\mathrm{CD_{iso}}| = 0.29$), characterized by a strong positive exciton couplet between 480 and 720 nm, with maximum at 660 nm (g_{abs} front: $+1.4 \cdot 10^{-2}$; back: $+1.1 \cdot 10^{-2}$) and 566 nm (g_{abs} front: $-5.3 \cdot 10^{-3}$; back: $-1.1 \cdot 10^{-2}$). In the case of DPP dye **3**, spin coating technique seems to start off an alternative aggregation pathway with respect to drop casting, two pathways which do not re-join even after annealing. This consideration was confirmed by the ECD spectrum of **SC-3** after thermal annealing (Figure 5h), where the relative weight of CD_{iso} and LDLB to the global ECD spectrum remained very similar ($\int|\mathrm{LDLB}|/\int|\mathrm{CD_{iso}}| = 0.34$), but minor changes in the spectral shape and especially the sign of LDLB were observed with respect to pristine **SC-3**, indicating some structural reorganization at different hierarchical levels. However, upon solvent annealing we observed a sharp change in the ECD spectrum of **SC-3**, with a general decrease in the intensity of dichroic signals (Figure 5g): in particular, if the shape of CD_{iso} remained unchanged, an increase of the LDLB term was found ($\int|\mathrm{LDLB}|/\int|\mathrm{CD_{iso}}| = 1.30$), resulting in significantly different profiles for the two faces of the thin film. Therefore, we could hypothesize that the exposure of DPP molecules to solvent vapors breaks the mesoscopic order of pristine **SC-3** sample, favoring the preferential orientation of local domains with respect to the glass slide surface responsible for a strong LDLB contribution. It is worth to emphasize that such aggregation mode showed a LDLB contribution of opposite sign with respect to pristine and solvent-annealed **DC-3** sample (Figure 5g vs. Figures 5b-c): this means that DPP dye **3** shows chiroptical properties in thin films which can be finely modulated depending on the deposition technique and post-deposition operations. Once again, ECD spectroscopy revealed its superior capability to provide valuable information on the possible co-existence of multiple aggregation pathways.

DPP dye **4** differs from the three previous compounds for: a) the presence of chiral groups on the terminal positions of the π-conjugated backbone, instead of on the lactam moieties of the central core; b) the use of (−)-menthyl bulky alkyl appendages, instead of (*S*)-3,7-dimethyl-1-octyl branched alkyl chains. Despite these differences, its optical and chiroptical characterization in thin films, depicted in Figure 6, offers some important food for thought. Interestingly, the absorbance spectrum of thin films prepared by drop casting (**DC-4**) (Figure 6a) was quite similar to that observed in 75% MeOH (that is, in condition of solution self-assembly), with a broad band between 455 nm and 780 nm (maximum at 661 nm) and a further band at higher energy (between 455 nm and 300 nm). The present result suggested the possibility that the solid-state

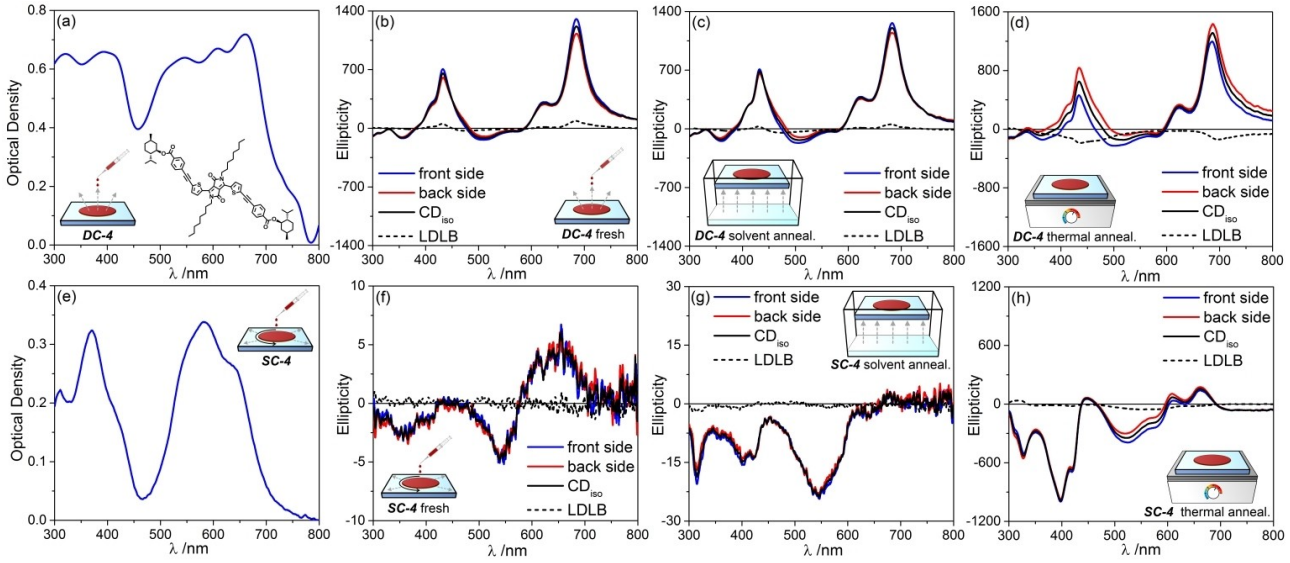

Figure 6. Optical and chiroptical investigation of the aggregation modes of chiral DPP dye **4** in thin films. Absorbance spectra recorded for: drop-casted sample **DC-4** (a); spin-coated sample **SC-4** (e). ECD spectra (normalized with respect to maximum absorbance) recorded for: drop-casted sample **DC-4** freshly prepared (b), after solvent annealing (c) and after thermal annealing (d); spin-coated sample **SC-4** freshly prepared (f), after solvent annealing (g) and after thermal annealing (h). For each panel: blue line is the ECD spectrum recorded for the front face; red line is the ECD spectrum recorded for the back face; black continuous line is the front-back semi-sum, i.e., calculated CD_{iso} contribution; black dashed line is the front-back semi-difference, i.e., calculated LDLB contribution.

structural organization in **DC-4** thin films was the same occurring in $CHCl_3$/MeOH mixtures. This was confirmed by ECD measurements (Figure 6b), where the spectral profile was similar to that of the same compound in 75% MeOH. In particular, in this case we observed a perfect overlapping of profiles recorded for the two faces of **DC-4**, indicating a pure reciprocal CD_{iso} contribution ($\int|LDLB|/\int|CD_{iso}| = 0.08$): two positive bands are present, with maximum at 684 nm (g_{abs} front: $+4.7\cdot10^{-2}$; back: $+4.2\cdot10^{-2}$) and 432 nm (g_{abs} front: $+2.7\cdot10^{-2}$; back: $+2.4\cdot10^{-2}$). Such structural order definitely represents a thermodynamically stable aggregation mode: in fact, post-deposition operations such as solvent annealing (Figure 6c) or thermal annealing (Figure 6d) did not impact on the chiroptical features of **DC-4**, and therefore on its solid-state organization at different hierarchical levels.

A totally different situation was observed in thin films fabricated by spin coating (**SC-4**). A first clue came from absorbance spectrum (Figure 6e), which is quite different from that recorded for **DC-4** sample: the main band fell between 460 nm and 730 nm, with maximum at 583 nm, and a further band was observed at 369 nm. Interestingly, such spectrum roughly recalls the absorbance spectrum of DPP dye **4** in pure $CHCl_3$ solution, rather than that in 75% MeOH: in the **SC-4** sample, DPP dye **4** seems to be in the condition of molecularly dispersed non-aggregated species. This was confirmed also by ECD measurements: freshly prepared samples (Figure 6f) showed only weak signals. It is clear that, in the present case, molecules of DPP **4** have not enough time to self-assemble into a structurally ordered aggregation mode before solvent evaporation: post-deposition operations were here key to reach a more stable solid-state organization. The effect of solvent annealing on the chiroptical features of **SC-4** was only marginal: a limited increase of the ECD signals was observed (Figure 6g), with a perfect correspondence of the profiles recorded for the two faces of **SC-4** ($\int|LDLB|/\int|CD_{iso}| = 0.07$), describing a set of structured, negative bands with maximum at 546 nm, 400 nm and 315 nm (g_{abs} front: $-9.9\cdot10^{-4}$; back: $-8.1\cdot10^{-4}$). The effect of solvent annealing on **SC-4** was instead highly impacting: a strong, mostly negative ECD spectrum appeared (Figure 6h), consisting of two structured bands with maxima at 521 nm and 398 nm (g_{abs} front: $-4.5\cdot10^{-2}$; back: $-4.5\cdot10^{-2}$). The strong CD_{iso} term ($\int|LDLB|/\int|CD_{iso}|$ ratio of 0.09), having opposite sign with respect to **DC-4**, suggested the formation of supramolecular aggregates with a very different structure. ECD spectra obtained after solvent and temperature annealing of **DC-4** are very similar to each other, and the same is true for **SC-4**. On the contrary, the two samples feature substantially different ECD profiles. This finding suggests that thermodynamically stable situations are reached in both cases, along two distinct aggregation pathways, which cannot be converted into each other.

A numerical comparison of the relevant chiroptical features of chiral DPP dyes **1–4** in thin films is depicted in the Table S1. We clearly demonstrated that these compounds can give rise to a manifold of situations. On the one hand, dichroic signals can be entirely due to the intrinsic chirality of the aggregates, responsible for a pure reciprocal CD_{iso} (this is the case of thin films of DPP dye **4** and, especially under specific conditions, also of compound **1**), or largely generated by the non-reciprocal LDLB contribution arising from the presence of highly anisotropic mesoscopic domains (as we found for the DPP **3**, especially fresh and solvent annealed **DC-3** samples and solvent

annealed **SC-3**). On the other hand, the intensity of ECD signals can be very weak (as in the case of thin films of compound **2**, due to its marked tendency to form achiral supramolecular aggregates), or very intense, with maximum dissymmetry factors g_{abs} up to almost 0.1 (in the case of pristine **DC-3** and **DC-4** samples, as well as **SC-4** after thermal annealing), which is a very high value achieved only in few other samples of organic π-conjugated dyes.[8]

Conclusion

In conclusion, we have reported four new chiral DPP dyes **1**–**4**, functionalized with enantiopure alkyl groups from natural sources: the (*S*)-3,7-dimethyl-1-octyl branched alkyl chain on the lactam moieties of DPP core (compounds **1**–**3**) or the (−)-menthyl bulky alkyl appendage on the terminal positions of π-conjugated backbone (compound **4**). All the chiral π-conjugated dyes were easily synthesized in good yields, then their aggregation modes in conditions of solution aggregation and thin films were evaluated by absorbance and ECD spectroscopies. Measurements in solution were carried out on mixtures of a *good* solvent (i.e., $CHCl_3$) and a *poor* solvent (i.e., MeOH) at different ratio, offering a step-by-step snapshot of self-assembly processes. An extended investigation of aggregation modes in thin films was also performed, studying the effect of deposition technique (drop casting vs. spin coating) and post-deposition operations (freshly prepared samples vs. solvent annealed and thermal annealed samples) on the chiroptical features. We found that these dyes can give rise to a manifold of situations in terms of signal intensities, with dissymmetry factor g_{abs} values ranging from 10^{-5} to almost 0.1, and of reciprocal vs. non-reciprocal CP absorption contributions, ranging from a pure CD_{iso} to a predominant LDLB. Since the chiroptical features of chiral DPP derivatives have been only marginally investigated to date, especially as thin films, the present study highlights the possibility to obtain organic layers of chiral DPP dyes with outstanding chiroptical features in terms of g_{abs} values and non-reciprocal properties. In this context, a further and deeper investigation is currently ongoing in our laboratories. In the flourishing field of chiral photonics and electronics, the development of thin films of π-conjugated dyes combining (very) large ECD signals with strong non-reciprocal CP absorption would have major implications, as it could open the way to their application as active layers in highly innovative optoelectronic devices, for example circularly polarized-organic field-effect transistors (CP-OFETs) able to discriminate the direction of sample illumination.

Experimental Section

Synthesis

General: (*S*)-Citronellyl bromide (**6**) was synthesized according to a literature procedure[20a, 34] starting from (*S*)-β-citronellol, available from Sigma-Aldrich by chemical synthesis at >97% purity. (1*R*,2*S*,5*R*)-2-isopropyl-5-methylcyclohexyl 4-iodobenzoate (**8**) was synthesized according to a literature procedure[39] starting from L-(−)-menthol, available from Sigma-Aldrich by chemical synthesis at >99% purity. 3,6-Bis(5-bromothiophen-2-yl)-2,5-dioctylpyrrolo[3,4-*c*]pyrrole-1,4(2*H*,5*H*)-dione (**12**) was synthesized according to a literature procedure.[40] All the other reagents were purchased at the highest commercial quality from Sigma-Aldrich and used without further purification. Solvents were purified by conventional methods, distilled and stored under argon. Preparative column chromatography was carried out using Macherey-Nagel silica gel (60, particle size 0.063–0.2 mm). Macherey-Nagel aluminum sheets with silica gel 60 F254 were used for TLC analyses. New compounds were characterized by ^{1}H NMR, ^{13}C NMR and LC–MS analysis. ^{1}H NMR and ^{13}C NMR spectra were acquired on an Agilent 500 spectrometer at 500 and at 126 MHz, respectively, using the $CDCl_3$ residual proton peak at δ = 7.26 ppm as internal standard for ^{1}H spectra and the signals of $CDCl_3$ at δ = 77.16 ppm as internal standard for ^{13}C spectra. High-resolution mass spectra were acquired with a Shimadzu high-performance liquid chromatography ion trap time-of flight (LC-IT-TOF) mass spectrometer via direct infusion of the samples by using acetonitrile as the elution solvent (samples were dissolved in acetonitrile containing small amounts of tetrahydrofuran). Melting points were determined on a Reichert Microscope or on a Stuart Scientific Melting point apparatus SMP3.

2,5-Bis((*S*)-3,7-dimethyloctyl)-3,6-di(thiophen-2-yl)pyrrolo[3,4-*c*]pyrrole-1,4(2*H*,5*H*)-dione (7): Compound **7** was synthesized according to a modified literature procedure.[26a] 3,6-Di(thiophen-2-yl)pyrrolo[3,4-*c*]pyrrole-1,4(2*H*,5*H*)-dione (**5**) (2.0 g, 6.66 mmol), (*S*)-1-bromo-3,7-dimethyloctane (**6**), (4.86 g, 21.98 mmol) and K_2CO_3 (3.04 g, 21.98 mmol) were dissolved in anhydrous and degassed DMF (40 mL). Catalytic amount of 18-crown-6 (30 mg, 0.11 mmol) was added and the mixture was stirred at 130 °C for 20 h. The reaction mixture was cooled to room temperature, quenched with a 10% aqueous solution of NaCl (100 mL) and extracted with CH_2Cl_2 (3×70 mL). The combined organic extracts were washed with a 10% aqueous solution of NaCl (3×50 mL), dried with Na_2SO_4, and concentrated under vacuum. The crude product was purified by washing with hexane leading to **7** as a dark purple solid (2.36 g, 61% yield). Spectroscopic data agree with those previously reported in the literature.[26a] **^{1}H NMR** (500 MHz, $CDCl_3$), δ (ppm): 8.90 (dd, *J* = 3.9, 1.1 Hz, 2H), 7.63 (dd, *J* = 5.0, 1.1 Hz, 2H), 7.28 (dd, *J* = 5.0, 3.9 Hz, 2H), 4.18–4.03 (m, 4H), 1.79–1.71 (m, 2H), 1.63–1.46 (m, 6H), 1.38–1.10 (m, 12H), 1.00 (d, *J* = 6.4 Hz, 6H), 0.85 (d, *J* = 6.6 Hz, 12H).

2,5-Bis((*S*)-3,7-dimethyloctyl)-3,6-bis(5-phenylthiophen-2-yl)pyrrolo[3,4-*c*]pyrrole-1,4(2*H*,5*H*)-dione (1): A Schlenk tube (2.5 cm) with a screw cap and equipped with a magnetic stirrer was charged with **7** (100 mg, 0.17 mmol), bromobenzene (68 mg, 0.43 mmol), anhydrous K_2CO_3 (59 mg, 0.43 mmol), pivalic acid (5 mg, 0.05 mmol), $Pd(OAc)_2$ (2.3 mg, 0.01 mmol) and DMA (2 mL) under a nitrogen atmosphere. The resulting mixture was reacted at 110 °C under magnetic stirring. After 2 h, the mixture was cooled to room temperature, poured into a 10% aqueous solution of NaCl (50 mL) and extracted with CH_2Cl_2 (3×50 mL). The combined organic layer was washed with a 10% aqueous solution of NaCl (2×50 mL), dried with Na_2SO_4 and concentrated under vacuum. Purification by column chromatography on silica gel (CH_2Cl_2/*n*-hexane = 2:1) afforded compound **1** (73 mg, 58% yield) as a dark purple solid, m. p. = 209–211 °C. **^{1}H NMR** (500 MHz, $CDCl_3$), δ (ppm): 8.96 (d, *J* = 4.1 Hz, 2H), 7.66 (d, *J* = 7.4 Hz, 4H), 7.46 (d, *J* = 4.1 Hz, 2H), 7.42 (t like, *J* = 7.5 Hz, 4H), 7.35 (t like, *J* = 7.3 Hz, 2H), 4.43–4.06 (m, 4H), 1.86–1.76 (m, 2H), 1.68–1.59 (m, 4H), 1.56–1.46 (m, 2H), 1.43–1.12 (m, 12H), 1.05 (d, *J* = 6.3 Hz, 6H), 0.84 (d, *J* = 6.6 Hz, 12H). **^{13}C NMR** (125 MHz, $CDCl_3$), δ (ppm): 161.4, 149.9, 139.6, 136.8, 133.3, 129.3, 129.0, 128.9, 126.3, 124.7, 108.2, 41.1, 39.4, 37.4, 37.0, 31.5, 28.1, 24.9, 22.8, 22.8, 19.8. **HR-MS** (LC–IT-TOF) *m*/*z*: calcd. for

$C_{46}H_{56}N_2O_2S_2$ $[M+H]^+$ 733.3856, found 733.3866, mass error = 1.36 ppm.

2,5-Bis((*S*)-3,7-dimethyloctyl)-3,6-bis(5-(4-(1,2,2-triphenylvinyl)phenyl) thiophen-2-yl)pyrrolo[3,4-*c*]pyrrole-1,4(2*H*,5*H*)-dione (2): A Schlenk tube (2.5 cm) with a screw cap and equipped with a magnetic stirrer was charged with **7** (116 mg, 0.20 mmol), (2-(4-bromophenyl)ethene-1,1,2-triyl)tribenzene (206 mg, 0.50 mmol), anhydrous K_2CO_3 (69 mg, 0.50 mmol), pivalic acid (21 mg, 0.20 mmol), $Pd(OAc)_2$ (5 mg, 0.02 mmol) and DMA (3 mL) under a nitrogen atmosphere. The resulting mixture was reacted at 110 °C under magnetic stirring. After 2.5 h, the mixture was cooled to room temperature, poured into a 10% aqueous solution of NaCl (50 mL) and extracted with CH_2Cl_2 (3×60 mL). The combined organic layer was washed with a 10% aqueous solution of NaCl (2×50 mL), dried with Na_2SO_4 and concentrated under vacuum. Purification by column chromatography on silica gel (CH_2Cl_2/*n*-hexane = 2:1) afforded compound **2** (175 mg, 70% yield) as a dark blue-purple solid, m. p. = 128–131 °C. **^{1}H NMR** (500 MHz, $CDCl_3$), δ (ppm): 8.92 (d, *J* = 4.1 Hz, 2H), 7.41 (d, *J* = 8.3 Hz, 4H), 7.38 (d, *J* = 4.1 Hz, 2H), 7.17–7.01 (m, 34H), 4.20–4.05 (m, 4H), 1.82–1.73 (m, 2H), 1.65–1.55 (m, 4H), 1.53–1.44 (m, 2H), 1.40–1.09 (m, 12H), 1.02 (d, *J* = 6.2 Hz, 6H), 0.82 (d, *J* = 6.6 Hz, 12H). **^{13}C NMR** (125 MHz, $CDCl_3$), δ (ppm): 161.4, 149.8, 144.8, 143.7, 143.6, 143.5, 141.9, 140.2, 139.5, 136.8, 132.3, 131.5, 131.5, 131.4, 131.1, 128.6, 128.1, 128.0, 127.8, 126.9, 126.8, 126.7, 125.4, 124.6, 108.2, 41.0, 39.4, 37.4, 37.0, 31.4, 28.1, 24.9, 22.8, 22.8, 19.7. **HR-MS** (LC-IT-TOF) *m/z*: calcd. for $C_{86}H_{84}N_2O_2S_2$ $[M+Na]^+$ 1263.5866, found 1263.5874, mass error = 0.63 ppm.

2,5-Bis((*S*)-3,7-dimethyloctyl)-3,6-bis(5-(4-(diphenylamino)phenyl) thiophen-2-yl)pyrrolo[3,4-*c*]pyrrole-1,4(2*H*,5*H*)-dione (3): A Schlenk tube (2.5 cm) with a screw cap and equipped with a magnetic stirrer was charged with **7** (116 mg, 0.20 mmol), 4-bromo-*N*,*N*-diphenylaniline (206 mg, 0.63 mmol), anhydrous K_2CO_3 (69 mg, 0.50 mmol), pivalic acid (21 mg, 0.20 mmol), $Pd(OAc)_2$ (5 mg, 0.02 mmol) and DMA (3 mL) under a nitrogen atmosphere. The resulting mixture was reacted at 110 °C under magnetic stirring. After 3 h, the mixture was cooled to room temperature, poured into a 10% aqueous solution of NaCl (50 mL) and extracted with CH_2Cl_2 (3×60 mL). The combined organic layer was washed with a 10% aqueous solution of NaCl (2×50 mL), dried with Na_2SO_4 and concentrated under vacuum. Purification by column chromatography on silica gel (CH_2Cl_2/*n*-hexane = 2:1) afforded compound **3** (142 mg, 66% yield) as a dark blue-purple solid, m. p. = 241–243 °C. **^{1}H NMR** (500 MHz, $CDCl_3$), δ (ppm): 8.98 (br s, 2H), 7.52 (d, *J* = 8.4 Hz, 4H), 7.37 (d, *J* = 4.1 Hz, 2H), 7.32–7.25 (m, 8H), 7.16–7.12 (m, 8H), 7.11–7.05 (m, 8H), 4.24–4.06 (m, 4H), 1.85–1.76 (m, 2H), 1.67–1.57 (m, 4H), 1.53–1.44 (m, 2H), 1.43–1.09 (m, 12H), 1.03 (d, *J* = 6.2 Hz, 6H), 0.82 (d, *J* = 6.6 Hz, 12H). **^{13}C NMR** (125 MHz, $CDCl_3$), δ (ppm): 161.5, 150.0, 148.7, 147.2, 139.4, 137.0, 129.6, 127.8, 127.1, 126.7, 125.2, 123.9, 123.7, 122.9, 108.0, 41.1, 39.4, 37.4, 37.0, 31.5, 28.1, 24.9, 22.8, 22.8, 19.8. **HR-MS** (LC-IT-TOF) *m/z*: calcd. for $C_{70}H_{74}N_4O_2S_2$ $[M+Na]^+$ 1089.5145, found 1089.5139, mass error = −0.55 ppm.

(1*R*,2*S*,5*R*)-2-Isopropyl-5-methylcyclohexyl 4-((trimethylsilyl)ethynyl) benzoate (10): Compound **10** was synthesized according to a modified literature procedure.[45] (1*R*,2*S*,5*R*)-2-Isopropyl-5-methylcyclohexyl 4-iodobenzoate (**8**) (100 mg, 0.26 mmol), $PdCl_2(PPh_3)_2$ (6 mg, $8.5\cdot10^{-3}$ mmol) and CuI (3 mg, 0.015 mmol) were dissolved in trimethylamine (5 mL) and THF (5 mL). The solution was degassed by bubbling N_2 for 10 minutes, then trimethylsilylacetylene (**9**) (100 μL, 0.72 mmol) was added. The resulting mixture was left under stirring at room temperature for 6 h, then it was hydrolyzed with a saturated ammonium chloride solution (50 mL) and extracted with AcOEt (3×50 mL). The combined organic layer was washed with water (3×50 mL), dried with Na_2SO_4 and concentrated under vacuum. Purification by column chromatography on silica gel (*n*-hexane) afforded compound **10** (83 mg, 90% yield) as a yellowish oil. Spectroscopic data agree with those previously reported in the literature.[45] **^{1}H NMR** (500 MHz, $CDCl_3$), δ (ppm): 7.96 (d, *J* = 8.4 Hz, 2H), 7.50 (d, *J* = 8.4 Hz, 2H), 4.92 (td, *J* = 10.9, 4.4 Hz, 1H), 2.15–2.08 (m, 1H), 1.98–1.89 (m, 1H), 1.76–1.69 (m, 2H), 1.60–1.50 (m, 2H), 1.18–1.05 (m. 2H), 0.97–0.87 (m, 7H), 0.79 (d, *J* = 7.0 Hz, 3H), 0.26 (s, 9H).

(1*R*,2*S*,5*R*)-2-Isopropyl-5-methylcyclohexyl 4-ethynylbenzoate (11): Compound **11** was synthesized according to a modified literature.[45] (1*R*,2*S*,5*R*)-2-Isopropyl-5-methylcyclohexyl 4-((trimethylsilyl)ethynyl)benzoate (**10**) (83 mg, 0.23 mmol) and tetrabutylammonium fluoride trihydrate (726 mg, 2.3 mmol) were dissolved in THF (15 mL). The resulting mixture was left under stirring at room temperature for 1 h, then it was hydrolyzed with a saturated ammonium chloride solution (50 mL) and extracted with CH_2Cl_2 (3× 50 mL). The combined organic layer was washed with water (3× 50 mL), dried with Na_2SO_4 and concentrated under vacuum. Purification by column chromatography on silica gel (*n*-hexane) afforded compound **11** (62 mg, 95% yield) as a yellowish oil. Spectroscopic data agree with those previously reported in the literature.[45] **^{1}H NMR** (500 MHz, $CDCl_3$), δ (ppm): 7.96 (d, *J* = 8.3 Hz, 2H), 7.51 (d, *J* = 8.3 Hz, 2H), 4.89 (td, *J* = 10.9, 4.4 Hz, 1H), 3.20 (s, 1H), 2.11–2.05 (m, 1H), 1.95–1.85 (m, 1H), 1.73–1.66 (m, 2H), 1.56–1.47 (m, 2H), 1.14–1.02 (m, 2H), 0.94–0.84 (m, 7H), 0.75 (d, *J* = 7.0 Hz, 3H).

Bis((1*R*,2*S*,5*R*)-2-isopropyl-5-methylcyclohexyl) 4,4′-((5,5′-(2,5-dioctyl-3,6-dioxo-2,3,5,6-tetrahydropyrrolo[3,4-*c*]pyrrole-1,4-diyl)bis(thiophene-5,2-diyl))bis(ethyne-2,1-diyl))dibenzoate (4): 3,6-Bis(5-bromothiophen-2-yl)-2,5-dioctylpyrrolo[3,4-*c*]pyrrole-1,4(2*H*,5*H*)-dione (**12**) (75 mg, 0.11 mmol), $PdCl_2(PPh_3)_2$ (4 mg, $5.7\cdot10^{-3}$ mmol) and CuI (3 mg, 0.015 mmol) were dissolved in trimethylamine (5 mL) and THF (5 mL). The solution was degassed by bubbling N_2 for 10 minutes, then (1*R*,2*S*,5*R*)-2-Isopropyl-5-methylcyclohexyl 4-ethynylbenzoate (**11**) (78 mg, 0.27 mmol) was added. The resulting mixture was left under stirring at 70 °C for 3 h, then it was hydrolyzed with a saturated ammonium chloride solution (50 mL) and extracted with CH_2Cl_2 (3×50 mL). The combined organic layer was washed with water (3×50 mL), dried with Na_2SO_4 and concentrated under vacuum. Purification by column chromatography on silica gel (*n*-hexane/ CH_2Cl_2/AcOEt = 9:1:1→CH_2Cl_2/AcOEt = 1:1) afforded compound **4** (75 mg, 63% yield) as a dark purple solid, m. p. = 170–172 °C. **^{1}H NMR** (500 MHz, $CDCl_3$), δ (ppm): 8.95 (d, *J* = 4.1 Hz, 2H), 8.05 (d, *J* = 8.3 Hz, 4H), 7.60 (d, *J* = 8.3 Hz, 4H), 7.44 (d, *J* = 4.1 Hz, 2H), 4.95 (td, *J* = 10.9, 4.4 Hz, 2H), 4.08 (t, *J* = 7.8 Hz, 4H), 2.17–2.10 (m, 2H), 2.01–1.91 (m, 2H), 1.80–1.71 (m, 8H), 1.61–1.53 (m, 4H), 1.48–1.41 (m, 4H), 1.40–1.22 (m, 16H), 1.20–1.07 (m, 4H), 0.99–0.90 (m, 14H), 0.87 (t, *J* = 6.9 Hz, 6H), 0.81 (d, *J* = 6.9 Hz, 6H). **^{13}C NMR** (125 MHz, $CDCl_3$), δ (ppm): 165.5, 161.3, 139.3, 135.7, 133.8, 131.5, 131.2, 131.1, 129.8, 128.2, 126.7, 109.1, 97.2, 85.0, 75.4, 47.4, 42.6, 41.1, 34.5, 31.9, 31.6, 30.2, 29.3, 27.0, 26.7, 23.8, 22.8, 22.2, 20.9, 16.7, 14.3 (one coincident peak not observed). **HR-MS** (LC-IT-TOF) *m/z*: calcd. for $C_{68}H_{84}N_2O_6S_2$ $[M]^+$ 1088.5765, found 1088.5774, mass error = 0.83 ppm.

Characterization

Solution aggregates: Stock solutions of each dye in $CHCl_3$ were typically 1.0 10^{-3} M, while working solutions in $CHCl_3$/MeOH mixtures were $1.3\cdot10^{-5}$ M. absorbance spectra were recorded at room temperature with a Jasco V-650 spectrophotometer, using a quartz cell. Electronic circular dichroism (ECD) spectra were recorded at room temperature with a Jasco J-710 spectropolarimeter, using a quartz cell.

Thin films: Drop casted samples were prepared by depositing dropwise on a quartz plate ~200 μL of a $2.0 \cdot 10^{-3}$ M solution of the dye (**1**, **3** and **4** in CH_2Cl_2; **2** in $CHCl_3$), followed by slow evaporation in an atmosphere saturated with solvent vapours. Spin coated samples were prepared by spin coating ~100 μL of a $2.0 \cdot 10^{-2}$ M solution of the dye (**1**, **3** and **4** in CH_2Cl_2; **2** in $CHCl_3$) on a quartz plate, using a WS-650MZ-23NPPB (Laurell Technologies Corp., North Wales, PA, USA) spin-coater; conditions: 1000 rpm, 30 sec, acceleration 1000 rpm/sec. Solvent annealing was carried out by keeping samples for 1 h in a closed chamber saturated with solvent vapours (CH_2Cl_2 in the case of **1**, **3** and **4**; $CHCl_3$ in the case of **2**). Thermal annealing was carried out by keeping samples for 1 h in an oven at high temperature (150 °C in the case of **1**, **3** and **4**; 100 °C in the case of **2**). Absorbance spectra were recorded at room temperature using a Jasco V-650 spectrophotometer. Electronic circular dichroism (ECD) spectra were recorded at room temperature using a Jasco J-710 spectropolarimeter. In all cases, at least 3 independent thin film samples were prepared and subjected to full absorbance and ECD analysis. In the first place, invariance of ECD upon sample rotation was testified, by rotating thin film sample by 90°, 180° and 270° around the optical axis: in no cases were found significant variations. For each sample, then, two ECD measurements were recorded: one with the organic layer facing the light source (front) and one with the organic layer facing the detector (back). Each ECD spectrum was normalized with respect to maximum absorbance to avoid any mistake possibly associated to sample inhomogeneity. The semi-sum and semi-difference of front and back ECD spectra were calculated in order to obtain reciprocal CD_{iso} and non-reciprocal LDLB contributions, according to Equations (1) and (2).

Computational details

DFT and TDDFT calculations were run with Gaussian'16,[46] with default grids and convergence criteria. A truncated model of **1** was employed where the *N*-alkyl chains were placed by *N*-methyl groups. Two starting structures of the model, with the thiophene-DPP bonds in s-cis and s-trans conformation, were optimized with DFT method using ωB97X-$>$D functional and 6-31$+$G(d) basis set in vacuo. TDDFT calculations were run on the DFT-optimized structure for the lowest-energy s-cis isomer using the CAM-B3LYP and B3LYP functionals and the def2-TZVP basis set, including 36 excited states. Electron/hole distribution isosurfaces were plotted with MutiWfn v3.8.[47] The same software was employed for estimating the Λ index.[48] The calculation results are summarized in the Supporting Information.

Acknowledgements

This work was financially supported by MIUR, Ministero dell' Istruzione, dell'Università e della Ricerca (PRIN 2017 project "CHIRALAB", Prot. 20172M3K5N) and Università di Pisa (PRA 2020_21). Open Access funding provided by Università degli Studi di Pisa within the CRUI-CARE Agreement.

Conflict of Interest

The authors declare no conflict of interest.

Data Availability Statement

The data that support the findings of this study are available from the corresponding author upon reasonable request.

Keywords: aggregation modes · diketopyrrolo[3,4-*c*]pyrroles · electronic circular dichroism · supramolecular chirality · thin films

[1] a) T. W. Kelley, P. F. Baude, C. Gerlach, D. E. Ender, D. Muyres, M. A. Haase, D. E. Vogel, S. D. Theiss, *Chem. Mater.* **2004**, *16*, 4413–4422; b) A. Facchetti, *Chem. Mater.* **2011**, *23*, 733–758; c) S. Casalini, F. Leonardi, C. A. Bortolotti, A. Operamolla, O. H. Omar, L. Paltrinieri, C. Albonetti, G. M. Farinola, F. Biscarini, *J. Mater. Chem.* **2012**, *22*, 12155–12163; d) O. Ostroverkhova, *Chem. Rev.* **2016**, *116*, 13279–13412; e) E. K. Lee, M. Y. Lee, C. H. Park, H. R. Lee, J. H. Oh, *Adv. Mater.* **2017**, *29*, 1703638; f) P. Friederich, A. Fediai, S. Kaiser, M. Konrad, N. Jung, W. Wenzel, *Adv. Mater.* **2019**, *31*, 1808256.

[2] a) W. Wu, Y. Liu, D. Zhu, *Chem. Soc. Rev.* **2010**, *39*, 1489–1502; b) C. Wang, H. Dong, W. Hu, Y. Liu, D. Zhu, *Chem. Rev.* **2012**, *112*, 2208–2267; c) A. Punzi, M. A. M. Capozzi, V. Fino, C. Carlucci, M. Suriano, E. Mesto, E. Schingaro, E. Orgiu, S. Bonacchi, T. Leydecker, P. Samorì, R. Musio, G. M. Farinola, *J. Mater. Chem. C* **2016**, *4*, 3138–3142; d) Y. H. Lee, M. Jang, M. Y. Lee, O. Y. Kweon, J. H. Oh, *Chem* **2017**, *3*, 724–763; e) S. N. Afraj, G.-Y. He, C.-Y. Lin, A. Velusamy, C.-Y. Huang, P.-S. Lin, S. Vegiraju, P.-Y. Huang, J.-S. Ni, S.-L. Yau, S.-H. Tung, T. Minari, C.-L. Liu, M.-C. Chen, *Adv. Mater. Technol.* **2021**, *6*, 2001028.

[3] a) U. Mitschke, P. Bäuerle, *J. Mater. Chem.* **2000**, *10*, 1471–1507; b) G. M. Farinola, R. Ragni, *Chem. Soc. Rev.* **2011**, *40*, 3467–3482; c) X.-K. Chen, D. Kim, J.-L. Brédas, *Acc. Chem. Res.* **2018**, *51*, 2215–2224; d) P. Tao, Y. Miao, H. Wang, B. Xu, Q. Zhao, *Chem. Rec.* **2019**, *19*, 1531–1561.

[4] a) J. Gierschner, J. Cornil, H.-J. Egelhaaf, *Adv. Mater.* **2007**, *19*, 173–191; b) J. Roncali, *Macromol. Rapid Commun.* **2007**, *28*, 1761–1775.

[5] a) J. Cornil, D. Beljonne, J.-P. Calbert, J.-L. Brédas, *Adv. Mater.* **2001**, *13*, 1053–1067; b) F. J. M. Hoeben, P. Jonkheijm, E. W. Meijer, A. P. H. J. Schenning, *Chem. Rev.* **2005**, *105*, 1491–1546; c) T. L. Andrew, T. M. Swager, *J. Polym. Sci. Part B* **2011**, *49*, 476–498.

[6] a) A. Salleo, R. J. Kline, D. M. DeLongchamp, M. L. Chabinyc, *Adv. Mater.* **2010**, *22*, 3812–3838; b) J. Rivnay, S. C. B. Mannsfeld, C. E. Miller, A. Salleo, M. F. Toney, *Chem. Rev.* **2012**, *112*, 5488–5519.

[7] a) P. A. Korevaar, T. F. A. de Greef, E. W. Meijer, *Chem. Mater.* **2014**, *26*, 576–586; b) Y. Dorca, E. E. Greciano, J. S. Valera, R. Gómez, L. Sánchez, *Chem. Eur. J.* **2019**, *25*, 5848–5864.

[8] G. Albano, G. Pescitelli, L. Di Bari, *Chem. Rev.* **2020**, *120*, 10145–10243.

[9] a) L. A. P. Kane-Maguire, G. G. Wallace, *Chem. Soc. Rev.* **2010**, *39*, 2545–2576; b) M. Verswyvel, G. Koeckelberghs, *Polym. Chem.* **2012**, *3*, 3203–3216; c) C. Resta, S. Di Pietro, M. Majerić Elenkov, Z. Hameršak, G. Pescitelli, L. Di Bari, *Macromolecules* **2014**, *47*, 4847–4850; d) M. Liu, L. Zhang, T. Wang, *Chem. Rev.* **2015**, *115*, 7304–7397.

[10] a) C. C. Lee, C. Grenier, E. W. Meijer, A. P. H. J. Schenning, *Chem. Soc. Rev.* **2009**, *38*, 671–683; b) Y. Yang, Y. Zhang, Z. Wei, *Adv. Mater.* **2013**, *25*, 6039–6049.

[11] a) J. R. Brandt, F. Salerno, M. J. Fuchter, *Nat. Chem. Rev.* **2017**, *1*, 0045; b) D.-W. Zhang, M. Li, C.-F. Chen, *Chem. Soc. Rev.* **2020**, *49*, 1331–1343.

[12] C. Train, M. Gruselle, M. Verdaguer, *Chem. Soc. Rev.* **2011**, *40*, 3297–3312.

[13] C. Wang, H. Fei, Y. Qiu, Y. Yang, Z. Wei, Y. Tian, Y. Chen, Y. Zhao, *Appl. Phys. Lett.* **1999**, *74*, 19–21.

[14] P. C. Mondal, C. Fontanesi, D. H. Waldeck, R. Naaman, *Acc. Chem. Res.* **2016**, *49*, 2560–2568.

[15] J. G. Ibanez, M. E. Rincón, S. Gutierrez-Granados, M. h. Chahma, O. A. Jaramillo-Quintero, B. A. Frontana-Uribe, *Chem. Rev.* **2018**, *118*, 4731–4816.

[16] a) N. Berova, L. D. Bari, G. Pescitelli, *Chem. Soc. Rev.* **2007**, *36*, 914–931; b) G. Pescitelli, L. Di Bari, N. Berova, *Chem. Soc. Rev.* **2011**, *40*, 4603–4625; c) G. Pescitelli, L. Di Bari, N. Berova, *Chem. Soc. Rev.* **2014**, *43*, 5211–5233; d) G. Pescitelli, *Chirality* **2022**, *34*, 333–363.

[17] a) M. Srebro-Hooper, J. Autschbach, *Annu. Rev. Phys. Chem.* **2017**, *68*, 399–420; b) R. Berardozzi, C. A. Guido, M. A. M. Capozzi, C. Cardellicchio, L. Di Bari, G. Pescitelli, *Eur. J. Org. Chem.* **2015**, *2015*, 5554–5562; c) M.

Górecki, F. Lipparini, G. Albano, T. Jávorfi, R. Hussain, G. Siligardi, G. Pescitelli, L. Di Bari, *Chem. Eur. J.* **2022**, *28*, e202103632.
[18] a) Y. Shindo, M. Nakagawa, *Rev. Sci. Instrum.* **1985**, *56*, 32–39; b) Y. Shindo, M. Nakagawa, Y. Ohmi, *Appl. Spectrosc.* **1985**, *39*, 860–868.
[19] a) A. Salij, R. H. Goldsmith, R. Tempelaar, *J. Am. Chem. Soc.* **2021**, *143*, 21519–21531; b) G. Albano, G. Pescitelli, L. Di Bari, *ChemNanoMat* **2022**, e202200219. DOI: 10.1002/cnma.202200219.
[20] a) G. Albano, M. Lissia, G. Pescitelli, L. A. Aronica, L. Di Bari, *Mater. Chem. Front.* **2017**, *1*, 2047–2056; b) G. Albano, F. Salerno, L. Portus, W. Porzio, L. A. Aronica, L. Di Bari, *ChemNanoMat* **2018**, *4*, 1059–1070; c) G. Albano, M. Górecki, G. Pescitelli, L. Di Bari, T. Jávorfi, R. Hussain, G. Siligardi, *New J. Chem.* **2019**, *43*, 14584–14593; d) G. Albano, L. A. Aronica, A. Minotto, F. Cacialli, L. Di Bari, *Chem. Eur. J.* **2020**, *26*, 16622–16627; e) F. Zinna, G. Albano, A. Taddeucci, T. Colli, L. A. Aronica, G. Pescitelli, L. Di Bari, *Adv. Mater.* **2020**, *32*, 2002575; f) O. Hassan Omar, M. Falcone, A. Operamolla, G. Albano, *New J. Chem.* **2021**, *45*, 12016–12023.
[21] M. Kaur, D. H. Choi, *Chem. Soc. Rev.* **2015**, *44*, 58–77.
[22] a) Z. Hao, A. Iqbal, *Chem. Soc. Rev.* **1997**, *26*, 203–213; b) O. Wallquist, R. Lenz, *Macromol. Symp.* **2002**, *187*, 617–630.
[23] M. Grzybowski, D. T. Gryko, *Adv. Opt. Mater.* **2015**, *3*, 280–320.
[24] a) C. B. Nielsen, M. Turbiez, I. McCulloch, *Adv. Mater.* **2013**, *25*, 1859–1880; b) W. Li, K. H. Hendriks, M. M. Wienk, R. A. J. Janssen, *Acc. Chem. Res.* **2016**, *49*, 78–85.
[25] W. Li, L. Wang, H. Tang, D. Cao, *Dyes Pigm.* **2019**, *162*, 934–950.
[26] a) M. Kirkus, L. Wang, S. Mothy, D. Beljonne, J. Cornil, R. A. J. Janssen, S. C. J. Meskers, *J. Phys. Chem. A* **2012**, *116*, 7927–7936; b) C. M. Mauck, P. E. Hartnett, E. A. Margulies, L. Ma, C. E. Miller, G. C. Schatz, T. J. Marks, M. R. Wasielewski, *J. Am. Chem. Soc.* **2016**, *138*, 11749–11761; c) N. Genevaz, P. Chávez, V. Untilova, A. Boeglin, C. Bailly, L. Karmazin, L. Biniek, *J. Mater. Chem. C* **2018**, *6*, 9140–9151; d) T. G. Hwang, J. Y. Kim, J. W. Namgoong, J. M. Lee, S. B. Yuk, S. H. Kim, J. P. Kim, *Photochem. Photobiol. Sci.* **2019**, *18*, 1064–1074.
[27] a) V. S. Gevaerts, E. M. Herzig, M. Kirkus, K. H. Hendriks, M. M. Wienk, J. Perlich, P. Müller-Buschbaum, R. A. J. Janssen, *Chem. Mater.* **2014**, *26*, 916–926; b) X. A. Jeanbourquin, A. Rahmanudin, A. Gasperini, E. Ripaud, X. Yu, M. Johnson, N. Guijarro, K. Sivula, *J. Mater. Chem. A* **2017**, *5*, 10526–10536.
[28] a) A. Punzi, E. Maiorano, F. Nicoletta, D. Blasi, A. Ardizzone, N. Ventosa, I. Ratera, J. Veciana, G. M. Farinola, *Eur. J. Org. Chem.* **2016**, *2016*, 2617–2627; b) A. Ardizzone, D. Blasi, D. Vona, A. Rosspeintner, A. Punzi, E. Altamura, N. Grimaldi, S. Sala, E. Vauthey, G. M. Farinola, I. Ratera, N. Ventosa, J. Veciana, *Chem. Eur. J.* **2018**, *24*, 11386–11392.
[29] A. Punzi, D. Blasi, A. Operamolla, R. Comparelli, G. Palazzo, G. M. Farinola, *RSC Adv.* **2021**, *11*, 11536–11540.
[30] K. Dhbaibi, L. Favereau, M. Srebro-Hooper, M. Jean, N. Vanthuyne, F. Zinna, B. Jamoussi, L. Di Bari, J. Autschbach, J. Crassous, *Chem. Sci.* **2018**, *9*, 735–742.
[31] T. Gao, Z. Jiang, B. Chen, Q. Sun, Y. Orooji, L. Huang, Z. Liu, *Dyes Pigm.* **2020**, *173*, 107998.
[32] P. A. Hume, J. P. Monks, F. Pop, E. S. Davies, R. C. I. MacKenzie, D. B. Amabilino, *Chem. Eur. J.* **2018**, *24*, 14461–14469.
[33] T. He, P. Leowanawat, C. Burschka, V. Stepanenko, M. Stolte, F. Würthner, *Adv. Mater.* **2018**, *30*, 1804032.
[34] G. Albano, T. Colli, T. Biver, L. A. Aronica, A. Pucci, *Dyes Pigm.* **2020**, *178*, 108368.
[35] M. Boukhris, M. S. J. Simmonds, S. Sayadi, M. Bouaziz, *Phytother. Res.* **2013**, *27*, 1206–1213.
[36] R. B. Croteau, E. M. Davis, K. L. Ringer, M. R. Wildung, *Naturwissenschaften* **2005**, *92*, 562.
[37] S. Zahn, T. M. Swager, *Angew. Chem. Int. Ed.* **2002**, *41*, 4225–4230; *Angew. Chem.* **2002**, *114*, 4399–4404.
[38] a) A. Punzi, M. A. M. Capozzi, S. Di Noja, R. Ragni, N. Zappimbulso, G. M. Farinola, *J. Org. Chem.* **2018**, *83*, 9312–9321; b) A. Punzi, N. Zappimbulso, G. M. Farinola, *Eur. J. Org. Chem.* **2020**, *2020*, 3229–3234; c) G. Albano, G. Decandia, M. A. M. Capozzi, N. Zappimbulso, A. Punzi, G. M. Farinola, *ChemSusChem* **2021**, *14*, 3391–3401; d) G. Albano, A. Punzi, M. A. M. Capozzi, G. Farinola, *Green Chem.* **2022**, *24*, 1809–1894.
[39] C. K. W. Jim, J. W. Y. Lam, C. W. T. Leung, A. Qin, F. Mahtab, B. Z. Tang, *Macromolecules* **2011**, *44*, 2427–2437.
[40] A. B. Tamayo, M. Tantiwiwat, B. Walker, T.-Q. Nguyen, *J. Phys. Chem. C* **2008**, *112*, 15543–15552.
[41] a) A. Tamayo, T. Kent, M. Tantitiwat, M. A. Dante, J. Rogers, T.-Q. Nguyen, *Energy Environ. Sci.* **2009**, *2*, 1180–1186; b) M. E. Farahat, H.-Y. Wei, M. A. Ibrahem, K. M. Boopathi, K.-H. Wei, C.-W. Chu, *RSC Adv.* **2014**, *4*, 9401–9411; c) D. Yang, F. Cheng, J. Zhang, H. Li, *Thin Solid Films* **2018**, *645*, 209–214.
[42] Z. Yang, Z. Chi, Z. Mao, Y. Zhang, S. Liu, J. Zhao, M. P. Aldred, Z. Chi, *Mater. Chem. Front.* **2018**, *2*, 861–890.
[43] G. Albano, L. A. Aronica, T. Biver, R. Detti, A. Pucci, *ChemistrySelect* **2018**, *3*, 1749–1754.
[44] C. Resta, G. Pescitelli, L. Di Bari, *Macromolecules* **2014**, *47*, 7052–7059.
[45] D. Müller, B. Frank, R. Beckert, H. Görls, *Z. Naturforsch. B* **2002**, *57*, 471–478.
[46] M. J. Frisch, G. W. Trucks, H. B. Schlegel, G. E. Scuseria, M. A. Robb, J. R. Cheeseman, G. Scalmani, V. Barone, G. A. Petersson, H. Nakatsuji, X. Li, M. Caricato, A. V. Marenich, J. Bloino, B. G. Janesko, R. Gomperts, B. Mennucci, H. P. Hratchian, J. V. Ortiz, A. F. Izmaylov, J. L. Sonnemberg, D. Williams-Young, F. Ding, F. LIpparini, F. Egidi, J. Goings, B. Peng, A. Petrone, T. Henderson, D. Ranasinghe, V. G. Zakrzewski, J. Gao, N. Rega, G. Zheng, W. Liang, M. Hada, M. Ehara, K. Toyota, R. Fukuda, J. Hasegawa, M. Ishida, T. Nakajima, Y. Honda, O. Kitao, H. Nakai, T. Vreven, K. Throssell, J. Montgomery, J. A., J. E. Peralta, F. Ogliaro, M. Bearpark, J. J. Heyd, E. Brothers, K. N. Kudin, V. N. Staroverov, T. A. Keith, R. Kobayashi, J. Normand, K. Raghavachari, A. Rendell, J. C. Burant, S. S. Iyengar, J. Tomasi, M. Cossi, J. M. Millam, M. Klene, C. Adamo, R. Cammi, J. W. Ochterski, R. L. Martin, K. Morokuma, O. Farkas, J. B. Foresman, D. J. Fox, Gaussian, Inc., Wallingford CT, **2016**.
[47] T. Lu, F. Chen, *J. Comput. Chem.* **2012**, *33*, 580–592.
[48] M. J. G. Peach, P. Benfield, T. Helgaker, D. J. Tozer, *J. Chem. Phys.* **2008**, *128*, 044118.

Manuscript received: April 16, 2022
Accepted manuscript online: June 8, 2022
Version of record online: July 26, 2022